JOURNAL OF COMPUTATIONAL PHYSICS **145,** 110–140 (1998)
ARTICLE NO. CP986023

Numerical Simulation of Unsteady Nonisothermal Capillary Interfaces

M. S. Hamed and J. M. Floryan

Department of Mechanical and Materials Engineering, University of Western Ontario, London, Ontario, Canada N6A 5B9
E-mail: mfloryan@eng-ntadmin.engga.uwo.ca

Received February 25, 1997; revised April 30, 1998

A family of algorithms for simulation of unsteady nonisothermal capillary interfaces has been developed. The algorithms are based on a coordinate transformation method. The time-dependent unknown physical domain is mapped onto a rectangular computational domain, with the explicit form of the mapping function not being known. Four types of temporal discretization are used leading to the first-order accurate one-step implicit method, second-order accurate Crank–Nicolson and trapezoidal methods and second-order accurate two-step implicit method. In all cases, second-order finite-difference approximations were used for spatial discretizations. Various tests demonstrated that the algorithms deliver theoretically predicted accuracy, even for very large interfacial distortions. The Crank–Nicolson and trapezoidal methods have been found to be conditionally stable and thus are not recommended.

1. INTRODUCTION

Zero gravity environment offers potential for development of novel material processing techniques. Control and optimization of many of these techniques critically depend on the complete understanding of all processes taking place in the liquid phase. Thermocapillary effect, which is gravity independent, is expected to play a dominant role. Understanding of the dynamics of nonisothermal interfaces (including their stability and existence limits) is, therefore, imperative. It is further of interest to determine how the response of an interface changes as a function of geometrical constraints and variations in heating strategies. The main objective of this work is to develop an algorithm capable of accurate prediction of the response of a capillary interface subject to an arbitrary time-dependent heating.

Variation of surface tension as a function of the temperature induces a tangential force along the interface which, in turn, generates motion in the adjacent phases. The shape of the interface results from the interaction between the surface tension and the pressure and

0021-9991/98 $25.00

normal viscous forces generated by the convection field. Analysis of the topology of the interface requires, therefore, determination of the solution of a free boundary problem for the Navier–Stokes and energy equations. Since it is an interplay between the surface tension gradients and the viscous stresses that dominates the dynamics of the system, these two effects have to be modelled very accurately.

Algorithms for free boundary problems for the Navier–Stokes equations have been reviewed by Floryan and Rasmussen [1]. The algorithms can be based on Eulerian, Lagrangian, and mixed formulations. Our present interest is in stability limits corresponding to a transition between steady and oscillatory convection and in early stages of the interface fragmentation problem. These problems are best dealt with using Eulerian formulation. The methods described in this paper rely on an analytical time-dependent mapping that transforms an unknown irregular physical domain into a fixed regular computational domain. The mapping function is unknown and has to be determined as part of the solution procedure. The steady algorithm developed by Chen and Floryan [2] is based on the same principles and can be viewed as a special case of the unsteady algorithms described in this paper.

Alternative approaches, which may involve either fixed grids or adaptive grids, were rejected for the reasons explained below. In the fixed grid approach, the interface travels through a fixed grid and this leads to difficulties in accurate determination of the location, orientation, and curvature of the interface between the grid points. The last two factors are crucial in our problem because they affect the modelling of normal viscous stress and surface tension effects at the interface. In the latter approach, the grid is generated numerically so that one of the grid lines always overlaps with the interface. Interfacial effects can be accurately modelled, but the cost of calculations may be high due to repetitive numerical coordinate generations. The analytical mapping technique selected here is optimal because it provides a sharp resolution of the interface and bypasses expensive numerical coordinate generation.

Shokoohi and Elrod [3, 4] used a coordinate mapping technique and streamfunction-vorticity formulation in the analysis of capillary breakup of a cylindrical jet. A special discretization technique was used which results in a high consumption of computing resources. The ADI solution technique provided first-order temporal accuracy. Loh and Rasmussen [5] coupled coordinate transformation with standard finite-difference discretization and studied flow in a cavity with the side wall moving. Primitive variables were used with a first-order discretization for time derivatives. Garba *et al.* [6] employed coordinate transformation, streamfunction-vorticity formulation, and spectral discretization in the analysis of two-dimensional flows infinite in one direction. Temporal discretizations with accuracies up to fourth order supplemented by stability analysis were given. Kang and Leal [7] coupled numerical coordinate generation, finite-difference discretization, streamfunction-vorticity formulation, and the ADI solution procedure in analysis of the deformation of bubbles. Chen *et al.* [8] used an approach based on coordinate generation and streamfunction-vorticity formulation in the analysis of thermocapillary convection in a rectangular cavity. Time derivatives were discretized using first-order two-point backward finite-difference formulas and the equations were solved using essentially a point relaxation procedure. The presented results were limited to small interface deformations only. No information pertaining to numerical error was given. Chen and Hwu [9] slightly modified the method given in [8] and used it for prediction of the transition from a steady to an oscillatory thermocapillary flow regime. Again, the results were limited to small interface deformations only.

In the present work, we focus our attention on the development of techniques for simulations of flows with large interfacial distortions. Geometry of the solution domain is regularized using a coordinate transformation method. The field equations are expressed in terms of streamfunction and vorticity. All spatial derivatives are discretized using second-order finite-difference discretization techniques. Different strategies applied to the discretization of time derivatives led to the first-order one-step implicit method, second-order Crank–Nicolson and trapezoidal methods, and a second-order two-step implicit method. These methods are compared with each other in terms of their accuracy, efficiency, and stability.

The paper is organized as follows. Section 2 discusses the model problem. Section 3 describes the numerical procedures. Coordinate transformation is defined in Section 3.1. Field equations expressed in terms of new independent variables are given in Section 3.2. The one-step implicit method is described in Section 3.3. The Crank–Nicolson method is discussed in Section 3.4. Section 3.5 is devoted to the trapezoidal method. The two-step implicit method is discussed in Section 3.6. A summary of the main conclusions is given in Section 4.

2. THE MODEL PROBLEM

Consider a rectangular cavity of length L and height H, as shown in Fig. 1. The upper surface, described by $y = h(x, t)$, is a free surface bounded by a passive gas of negligible density and viscosity. Temperature distribution in the gas $T = T_g(x, t)$ is assumed to be known. The motion of the liquid is described by variations of surface tension arising due to thermocapillary effect. The shape of the interface, which is a function of time, results from the instantaneous balance of forces at the interface. The contributing factors are the local value of the surface tension (which depends on the local temperature which, in turn, results from the overall energy transport) and the pressure and viscous stresses associated with the convection field. Physical motivation and the relevant scaling can be found in [10].

In the absence of body forces, the unsteady two-dimensional motion of the liquid is governed by the equations

$$u_x + v_y = 0, \quad \mathrm{Re}(u_t + uu_x + vu_y) = -p_x + u_{xx} + u_{yy}, \tag{1a), (1b}$$

$$\mathrm{Re}(v_t + uv_x + vv_y) = -p_y + v_{xx} + v_{yy}, \quad \mathrm{Ma}(T_t + uT_x + vT_y) = T_{xx} + T_{yy}, \tag{1c), (1d}$$

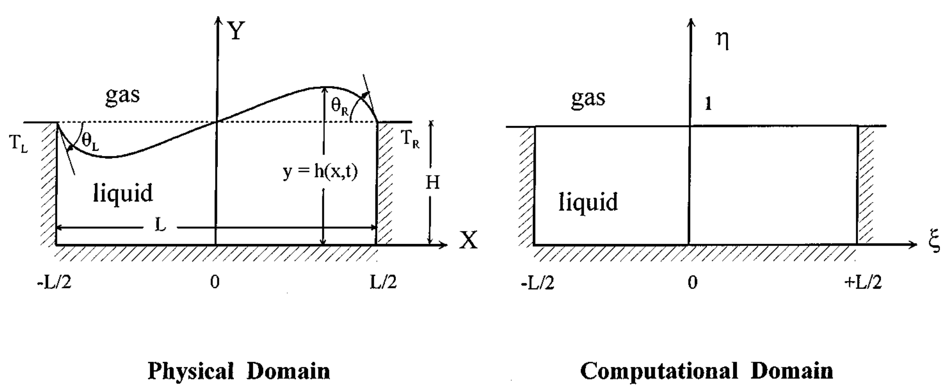

FIG. 1. Sketch of the model problem.

where u and v are respectively the x and y components of the velocity vector, p is the pressure, T is the temperature of the liquid, t stands for the time, Re and Ma are respectively the Reynolds and the Marangoni numbers, and subscripts x, y, t stand for $\partial/\partial x$, $\partial/\partial y$, and $\partial/\partial t$, respectively. These equations are subject to the following boundary conditions:

$$x = -\frac{1}{2}L: \quad u = v = 0, \quad T = T_L, \tag{2a}$$

$$x = \frac{1}{2}L: \quad u = v = 0, \quad T = T_R, \tag{2b}$$

$$y = 0: \quad u = v = T_y = 0, \tag{2c}$$

$$y = h(x,t): \quad h_t + uh_x = v, \tag{2d}$$

$$-p + 2\left[h_x^2 u_x + v_y - h_x(v_x + u_y)\right]\left(1 + h_x^2\right)^{-1} = \mathrm{Ca}^{-1}(1 - Ca\,T)h_{xx}\left(1 + h_x^2\right)^{-3/2}, \tag{2e}$$

$$2h_x(-u_x + v_y) + \left(1 - h_x^2\right)(v_x + u_y) = -(T_x + h_x T_y)\left(1 + h_x^2\right)^{1/2}, \tag{2f}$$

$$(-h_x T_x + T_y)\left(1 + h_x^2\right)^{-1/2} + \mathrm{Bi}[T - T_g(x,t)] = 0. \tag{2g}$$

In the above, Ca and Bi stand for the capillary and the Biot numbers, respectively. The left and right walls of the cavity are assumed to be isothermal and are kept at constant temperatures T_L and T_R, respectively. The bottom of the cavity is assumed to be adiabatic. Equation (2d) describes the kinematic condition at the interface, (2e) and (2f) describe the balance of the normal and tangential forces at the interface, respectively, and (2g) specifies a general heat transfer condition at the interface. Thermal conditions (2a) and (2b), and the temperature distribution in the gas phase $T_\mathrm{g}(x,t)$ in (2g), must satisfy the consistency conditions at the upper corners. The deforming interface must satisfy the mass conservation constraint

$$\int_{-1/2L}^{1/2L} h(x,t)\,dx = V. \tag{3}$$

The problem is closed by specifying the type of contact made by the interface at the end walls. Two cases will be considered:

(i) fixed contact points,

$$h(-1/2L) = 1, \quad h(1/2L) = 1; \tag{4a}$$

(ii) fixed contact angles (moving contact points),

$$h_x(-1/2L) = \tan\theta_L, \quad h_x(1/2L) = -\tan\theta_R. \tag{4b}$$

The type of the contact that may exist between the interface and the side walls has a very strong effect on the response of the flow system (see Section 3.3.3.2).

3. NUMERICAL METHOD

3.1. Coordinate Transformation

The flow problem (1)–(4) has to be solved numerically on an irregular, time-dependent solution domain (as defined by $h(x,t)$). Application of the transformation

$$\xi = x, \quad \eta = y/h(x,t) \tag{5}$$

maps this domain onto a fixed rectangular domain in the computational (ξ, η) plane (Fig. 1) permitting use of standard finite-difference discretization techniques for spatial derivatives. The explicit form of the mapping function $h(x,t)$ is not known and has to be determined as a part of the numerical procedure.

3.2. Streamfunction-Vorticity Formulation

The use of the streamfunction-vorticity formulation permits a simple enforcement of the incompressibility condition (1a) which is crucial in the case of a free boundary problem considered here. Field equations (1) take the form

$$\nabla^2\psi + \omega = 0, \tag{6a}$$

$$\omega_t - \eta h^{-1} h_t \omega_\eta + h^{-1}(\psi_\eta \omega_\xi - \psi_\xi \omega_\eta) = \nabla^2\omega/\mathrm{Re}, \tag{6b}$$

$$T_t - \eta h^{-1} h_t T_\eta + h^{-1}(\psi_\eta T_\xi - \psi_\xi T_\eta) = \nabla^2 T/\mathrm{Ma}, \tag{6c}$$

where

$$u = \psi_y, \quad v = -\psi_x, \quad \omega = v_x - u_y, \tag{6d}$$

$$\nabla^2 = \frac{\partial^2}{\partial\xi^2} - 2\eta h_\xi h^{-1}\frac{\partial^2}{\partial\xi\,\partial\eta} + h^{-2}\left(\eta^2 h_\xi^2 + 1\right)\frac{\partial^2}{\partial\eta^2} + \left(2h_\xi^2 - h h_{\xi\xi}\right)\eta h^{-2}\frac{\partial}{\partial\eta}.$$

The boundary conditions take the form

$$\xi = -1/2L: \quad \psi = \psi_\xi = 0, \quad T = T_L, \tag{6e}$$

$$\xi = 1/2L: \quad \psi = \psi_\xi = 0, \quad T = T_R, \tag{6f}$$

$$\eta = 0: \quad \psi = \psi_\eta = 0, \quad T_\eta = 0, \tag{6g}$$

$$\eta = 1: \quad h_t + \psi_\xi = 0, \tag{6h}$$

$$-p + 2\frac{\left(h_\xi\psi_{\xi\xi} - \left(1+h_\xi^2\right)h^{-1}\psi_{\xi\eta} + h_\xi h^{-2}\left(1 + h_\xi^2 - h h_{\xi\xi}\right)\psi_\eta\right)}{\left(1+h_\xi^2\right)}$$
$$= \mathrm{Ca}^{-1}(1 - Ca\,T)h_{\xi\xi}(1+h_\xi)^{-3/2}, \tag{6i}$$

$$-\left(1-h_\xi^2\right)\psi_{\xi\xi} + h^{-2}\left(1+h_\xi^2\right)^2\psi_{\eta\eta} - 2h_\xi h^{-1}\left(1+h_\xi^2\right)\psi_{\xi\eta} + \left[\left(1-h_\xi^2\right)h h_{\xi\xi}\right.$$
$$\left. + 2h_\xi^2\left(1+h_\xi^2\right)\right]h^{-2}\psi_\eta = -T_\xi\left(1+h_\xi^2\right)^{1/2}, \tag{6j}$$

$$\left(1+h_x^2\right)^{1/2}h^{-1}T_\eta - h_\xi\left(-1+h_\xi^2\right)^{-1/2}T_\xi + \mathrm{Bi}(T - T_g(\xi,t)) = 0. \tag{6k}$$

3.3. One-Step Implicit Method

It is assumed that all quantities are known at time $t = n\Delta t$ and that their values at $t = (n+1)\Delta t$ are sought. Here Δt is the length of the time step. Temperature $T_g(\xi, t)$ in the gas phase is changed to its value at $t = (n+1)\Delta t$ and the field equations are solved keeping the location of the interface and the value of the streamfunction at the interface unchanged and without enforcing the normal stress (6i) and the kinematic (6h) conditions. We shall refer to this problem as the inner problem or the inner solution. The normal stress condition is used subsequently to determine the new location of the interface and the kinematic condition is used to evaluate the new value of the stream function at the interface. We shall refer to this part of the solution process as the outer problem or the outer solution. The complete solution procedure involves iterations between the inner and the outer problems until all conditions are satisfied with the desired accuracy. We shall refer to the above iteration as the outer iteration. The flow chart illustrating this process is shown in Fig. 2. We shall begin the description of the algorithm with the description of the solution of the inner problem.

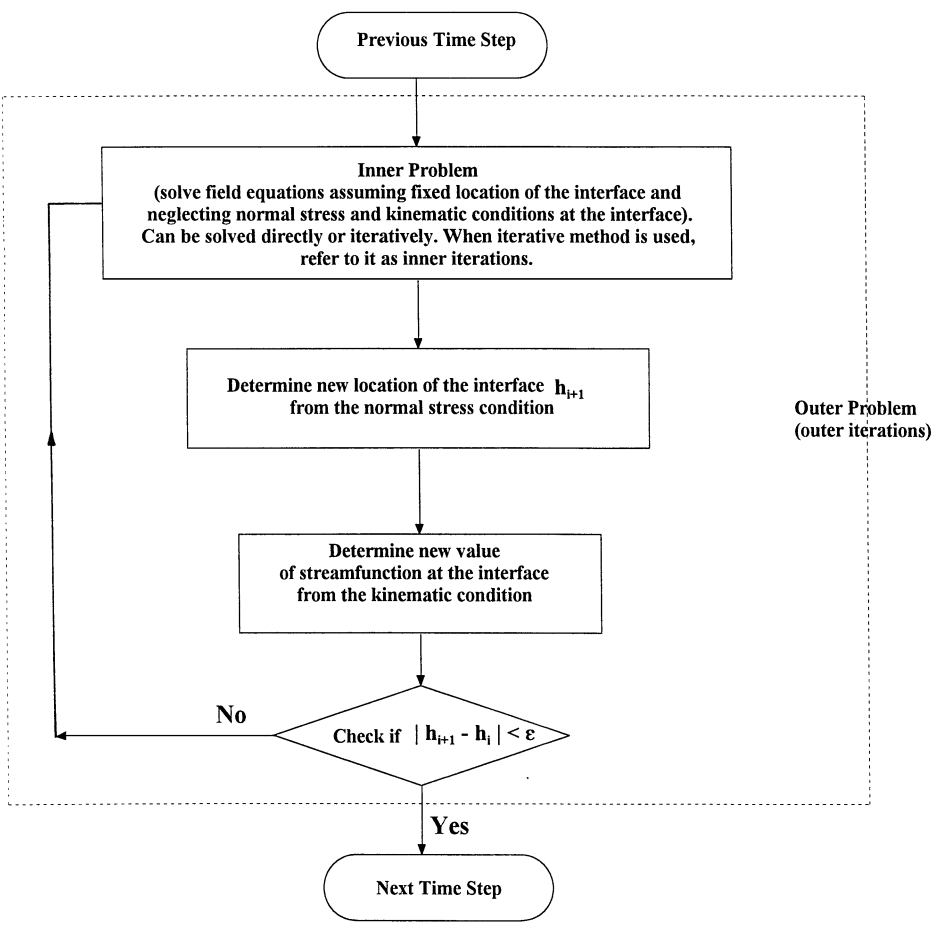

FIG. 2. Flow chart for the proposed algorithms.

3.3.1. *The Inner Problem*

The field equations are written at time $t = (n+1)\Delta t$ in the form

$$\nabla^2 \psi^{n+1} + \omega^{n+1} = 0, \tag{7a}$$

$$\frac{\omega^{n+1} - \omega^n}{\Delta t} + (h^{n+1})^{-1}\left(\psi_\eta^{n+1} \cdot \omega_\xi^{n+1} - \psi_\xi^{n+1} \cdot \omega_\xi^{n+1}\right)$$
$$+ \eta (h^{n+1})^{-1} \omega_\eta^{n+1}\left(\psi_\xi^{n+1}\right)_b - \nabla^2 \omega^{n+1}/\mathrm{Re} = 0, \tag{7b}$$

where ω_t^{n+1} has been replaced by backward, first-order finite-difference approximation, and h_t^{n+1} was replaced by $(\psi_\xi^{n+1})_b$ by taking advantage of the kinematic condition (6h). In the above, superscripts n and $n+1$ refer to the time steps, subscript b denotes the value of the field variable at the interface, and h^{n+1} is known from the previous outer iteration (or from the previous time step in the case of the first outer iteration). The energy transport equation has the same form as (7b) with ω^{n+1} is replaced by T^{n+1} and Re is replaced by Ma.

A rectangular computational grid of size $\Delta\xi$, $\Delta\eta$ in the ξ, η directions is considered, with grid lines parallel to the ξ and η axes and such that the grid fits exactly the geometry of the computational domain, with the side and bottom walls and the interface as certain grid lines. Around a typical interior grid point (ξ_0, η_0) we adopt the convention that quantities at (ξ_0, η_0) and eight neighbouring points are denoted by subscripts $0, 1, \ldots, 8$ as shown in Fig. 3. Equations (7) are written at each interior grid point and the spatial derivatives are approximated by using second-order finite-differences in the usual manner to give

$$-2(A_1 + A_2)\psi_0^{n+1} + A_1\psi_1^{n+1} - A_3\psi_2^{n+1} + (A_2 + A_4)\psi_3^{n+1} + A_3\psi_4^{n+1} + A_1\psi_5^{n+1}$$
$$- A_3\psi_6^{n+1} + (A_2 - A_4)\psi_7^{n+1} + A_3\psi_8^{n+1} + \omega_0^{n+1} = 0, \tag{8a}$$

$$-[2(A_1 + A_2) + \mathrm{Re}\, A_6]\omega_0^{n+1} + \left[A_1 - \mathrm{Re}\, A_5\left(\psi_3^{n+1} - \psi_7^{n+1}\right)\right]\omega_1^{n+1} - A_3\omega_2^{n+1}$$
$$+ \left[A_2 + A_4 - \mathrm{Re}\, A_7 + \mathrm{Re}\, A_5\left(\psi_1^{n+1} - \psi_5^{n+1}\right)\right]\omega_3^{n+1} + A_3\omega_4^{n+1}$$
$$+ \left[A_1 + \mathrm{Re}\, A_5\left(\psi_3^{n+1} - \psi_7^{n+1}\right)\right]\omega_5^{n+1} - A_3\omega_6^{n+1}$$
$$+ \left[A_2 - A_4 + \mathrm{Re}\, A_7 - \mathrm{Re}\, A_5\left(\psi_1^{n+1} - \psi_5^{n+1}\right)\right]\omega_7^{n+1} + A_3\omega_8^{n+1} + \mathrm{Re}\, A_6\omega_0^n = 0, \tag{8b}$$

where

$$A_1 = (\Delta\xi)^{-2}, \quad A_2 = \left[1 + \eta^2\left(h_\xi^{n+1}\right)^2\right](h^{n+1}\Delta\eta)^{-2}, \quad A_3 = \eta h_\xi^{n+1}(2h^{n+1}\Delta\xi\,\Delta\eta)^{-1},$$
$$A_4 = \eta\left[2\left(h_\xi^{n+1}\right)^2 - h^{n+1}h_{\xi\xi}^{n+1}\right][2(h^{n+1})^2\Delta\eta]^{-1}, \quad A_5 = (4h^{n+1}\Delta\xi\,\Delta\eta)^{-1},$$
$$A_6 = (\Delta t)^{-1}, \quad A_7 = \eta\left(\psi_\xi^{n+1}\right)_b(2h^{n+1}\Delta\eta)^{-1}.$$

The boundary conditions for (8) are given by (6e)–(6g), (6j). For (8a) the values of ψ^{n+1} are known at all grid points on the solid walls and are known from the previous outer iteration (or from the previous time step in the case of the first outer iteration) at the interface. For (8b) a boundary condition for $\omega^{\mathrm{n}+1}$ is required at the grid points on the side walls. Here, we use a second-order approximation for the side walls,

$$\omega_w^{n+1} = \left(\psi_{i+1}^{n+1} - 8\psi_i^{n+1}\right)/(2\Delta\xi^2), \tag{9a}$$

where subscript w refers to the wall values, subscript i refers to the internal grid point most immediate to w and subscript $(i+1)$ refers to the next grid point in the same direction. A similar formula for the bottom of the cavity has the form

$$\omega_w^{n+1} = \left(\psi_{i+1}^{n+1} - 8\psi_i^{n+1}\right)/[2\Delta\eta^2(h^{n+1})^2]. \tag{9b}$$

In the above, h^{n+1} is considered to be known from the previous outer iteration (or from the previous time step in the case of the first outer iteration). The boundary condition at the interface is obtained by substituting (6j) into (6a), resulting in

$$\omega_b^{n+1} = -2\left(1+\left(h_\xi^{n+1}\right)^2\right)^{-1}\left(\psi_{\xi\xi}^{n+1}\right)_b + (h^{n+1})^{-1}\left(1+\left(h_\xi^{n+1}\right)^2\right)^{-1} \times\left\{h^{n+1}\left(1+\left(h_\xi^{n+1}\right)^2\right)^{1/2}\left(T_\xi^{n+1}\right)_b + 2h_{\xi\xi}^{n+1}\left(\psi_\eta^{n+1}\right)_b\right\}. \tag{10}$$

The reader may note that the first term on the right-hand side of (10) arises due to unsteady effects. In the above $(\psi_{\xi\xi}^{n+1})_{\mathrm{b}}$, h^{n+1}, h_ξ^{n+1}, $h_{\xi\xi}^{n+1}$ are considered to be known; h_ξ^{n+1} and $h_{\xi\xi}^{n+1}$ are evaluated using standard central-difference approximations based on values of h^{n+1} from the previous outer iteration (or from the previous time step in the case of the first iteration). Evaluation of $(\psi_{\xi\xi}^{n+1})_b$ is discussed in Section 3.3.2.3. Temperature gradient $(T_\xi^{n+1})_b$ is evaluated using standard central-difference approximation and $(\psi_\eta^{n+1})_b$ is determined using one-sided difference approximation. All spatial discretization formulas are second-order accurate.

For the energy equation, values of T^{n+1} are known at the side walls. At the remaining two boundaries, T^{n+1} is determined from the discretized boundary conditions (6g) and (6k) using second-order finite-difference formulas.

Assuming that the location of the interface h^{n+1} and the value of the stream function ψ_b^{n+1} at the interface are known, the problem (7), supplemented by the energy equation and the boundary conditions described above, can be solved either directly or iteratively. In the present study, we have used different methods and applied them on computers of various architectures, including single processor sequential machines and multiprocessor vector machines. The following presentation is based on the Gauss–Seidel procedure, which is a good iterative reference method. Because of this choice, we shall refer to the solution of the inner problem as the inner iteration. Values from the last outer iteration (or the previous time step in the case of the first outer iteration) were used as an initial guess for the field variables. The systematic iterative procedure between the various equations consisted of

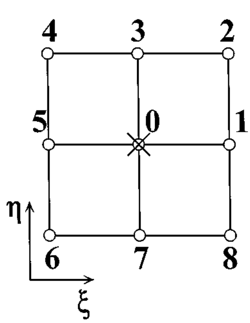

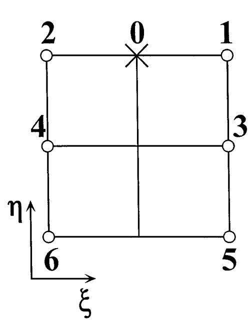

FIG. 3. Sketch of a typical computational module used in the interior of the solution domain.

FIG. 4. Sketch of a computational module used to evaluate $\psi_{\xi\eta}$ at the interface.

performing one complete Gauss–Seidel iteration of (7a), followed by a similar iteration of (7b) and then a complete iteration of the energy equation, followed by a recalculation of the boundary values of ω^{n+1} and T^{n+1}. The iterations were performed until the convergence criteria, $|q_{i+1} - q_i| < \varepsilon_1$ and $|\mathrm{Res}_i| < \varepsilon_1$ with $\varepsilon_1 = 10^{-5} - 10^{-7}$ were satisfied at all grid points. In the above, q stands for any of the flow quantities (ψ, ω, T), Res denotes residuum of any of the discretized field equations, and subscript i denotes the (inner) iteration number.

Since h^{n+1} and ψ_b^{n+1} are known only approximately, 20%–30% savings in computational time can be achieved by relaxing the convergence criterion to $\varepsilon_1 \approx 10^{-3}$ during the first outer iteration and decreasing it in stages to its prescribed value during the subsequent (outer) iterations. The condition for residuum of the vorticity transport equation was usually most difficult to satisfy. The relaxation factors used in the calculations varied from 1.0 for almost flat interfaces to 0.1 for very deformed interfaces. These factors had to be further reduced with increasing values of Re and Ma.

3.3.2. *Outer Problem*

The outer problem consists of evaluation of the new location of the interface and the new value of ψ_b^{n+1} that correspond to the most recent solution of the inner problem. The interface is determined from the normal stress condition (2e) subject to the contact conditions (4) and the volume constraint (3). The field variables determined by the inner problem are kept constant during solution of the outer problem.

3.3.2.1. *Evaluation of the pressure.* Normal stress condition (2e) involves the value of pressure at the interface which has to be determined on the basis of the known solution of the inner problem. Equations (1b)–(1c) are solved for components of the pressure gradient, transferred into the (ξ, η) plane using (5), expressed in a form suitable for the interface (i.e., for $\eta = 1$), and combined to yield

$$\begin{aligned} p_\xi = {} & h_\xi \omega_\xi - \left(1 + h_\xi^2\right) h^{-1} \omega_\eta - \mathrm{Re}\, h^{-2} \psi_\eta \left(\left(1 + h_\xi^2\right) \psi_{\xi\eta} + h_\xi h^{-1} \left(h_{\xi\xi} h - h_\xi^2 - 1\right) \psi_\eta\right) \\ & - \mathrm{Re}\left[\left(1 + h_\xi^2\right) h^{-1} \psi_{\eta t} - h_\xi \psi_{\xi t} + h^{-2} \psi_\eta \left[\left(1 + h_\xi^2\right) \psi_\xi - 2 h h_\xi \psi_{\xi\xi}\right]\right]. \end{aligned} \tag{11a}$$

The term in the square bracket arises due to unsteady effects. The reader may note that the above equation does not require knowledge of the pressure from the previous time step. Equation (11a) is integrated from $\xi = 0$ to $\xi = a$ to get

$$\tilde{p}(a) = (h_\xi \omega)_{\xi=a} - (h_\xi \omega)_{\xi=0} - \int_0^a h_{\xi\xi} \omega \, d\xi + \int_0^a B \, d\xi, \tag{11b}$$

where the first three terms on the right-hand side (RHS) resulted from the integration by parts of the first term on the RHS of (11a) and B stands for the remaining terms on the RHS of (11a). Integrals in (11b) are evaluated using the trapezoidal rule based on the same grid as used in the determination of the flow field. Direct numerical integration of (11a) is not advisable because it requires knowledge of the (undefined) values of vorticity at the contact points.

The expression for pressure can be written in general as

$$p(\xi, 1, t) = \tilde{p}(\xi, 1, t) + K(t), \tag{12}$$

where $\tilde{p}$ denotes normalized pressure satisfying condition $\tilde{p}(0, 1, t) = 0$ (i.e., it is described by (11b)), and $K(t)$ denotes an unknown additive constant.

The spatial derivatives with respect to η in (11a) are evaluated using one-sided second-order finite-difference approximations based on the grid used in the inner problem. Mixed derivative of ψ at $t = (n+1)\Delta t$ with respect to spatial coordinates $\psi_{\xi\eta}$ is evaluated at the interface according to

$$(\psi_{\xi\eta})_0 = [3(\psi_1 - \psi_2) - 4(\psi_3 - \psi_4) + \psi_5 - \psi_6]/(4\Delta\xi\,\Delta\eta) + O(\Delta\xi^2) + O(\Delta\eta^2), \quad (13)$$

where the subscripts refer to points shown in Fig. 4. Mixed derivatives of ψ with respect to space and time $\psi_{\xi t}$, $\psi_{\eta t}$ are calculated at the interface according to the formulas

$$\begin{aligned}(\psi_{\xi t})_0 &= \left[\psi_2^{n+1} - \psi_1^{n+1} - \psi_2^n + \psi_1^n\right]/(2\Delta\xi\,\Delta t) + O(\Delta t) + O(\Delta\xi^2),\\ (\psi_{\eta t})_0 &= \left[3\left(\psi_0^{n+1} - \psi_0^n\right) - 4\left(\psi_1^{n+1} - \psi_1^n\right) + \psi_2^{n+1} - \psi_2^n\right]/(2\Delta\eta\Delta t)\\ &\quad + O(\Delta t) + O(\Delta\eta^2),\end{aligned} \quad (14)$$

where the subscripts refer to grid points shown in Fig. 5. These formulas are first-order accurate in time and second-order accurate in space.

3.3.2.2. *Evaluation of the new location of the interface.* The normal stress condition (6i) can be interpreted as a nonlinear ordinary differential equation for $h(\xi)$ with the known variable coefficients expressed in terms of ψ^{n+1}, T^{n+1}, p^{n+1}. This equation involves unknown pressure normalization constant K and is subject to boundary conditions (4) and constraint (3). It is assumed that a sufficiently good approximation of the solution is available, i.e.,

$$h = h_o + h_1, \quad K = K_o + K_1, \quad (15)$$

where h_o, K_o are known and $h_1 \ll 1$, $K_1 \ll 1$. The Newton–Raphson linearization process

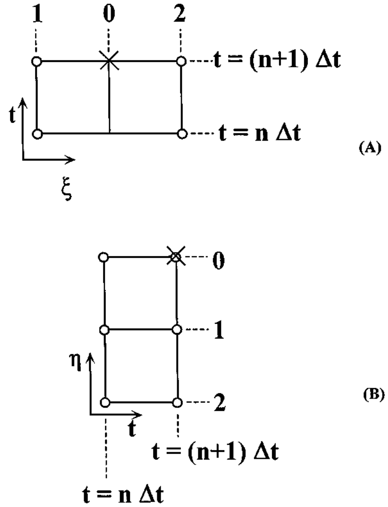

FIG. 5. Sketch of a computational module used to evaluate $\psi_{\xi t}$ (a) and $\psi_{\eta t}$ (b) at the interface in the one-step implicit method.

leads to the problem for h_1, K_1,

$$h_{1\xi\xi} + H(\xi)h_{1\xi} = M(\xi) + K_1 N(\xi), \tag{16a}$$

$$h_1(-1/2L) = 0 \quad \text{or} \quad h_{1\xi}(-1/2L) = 0, \tag{16b}$$

$$h_1(1/2L) = 0 \quad \text{or} \quad h_{1\xi}(1/2L) = 0, \tag{16c}$$

$$\int_{-1/2L}^{1/2L} h_1 \, d\xi = 0, \tag{16d}$$

where

$$\begin{aligned}
H(\xi) &= -3h_{o\xi}h_{o\xi\xi}\left(1+h_{o\xi}^2\right)^{-1} - \mathrm{Ca}(1-\ \mathrm{Ca}\,T)^{-1}\left(1+h_{o\xi}^2\right)^{-1/2} \\
&\quad \times \left[4\psi_{\xi\xi} - 4h_{o\xi\xi}h_o^{-1}\psi_\eta + 2\left(1+h_{o\xi}^2\right)\omega\right], \\
M(\xi) &= -\mathrm{Ca}(1-\ \mathrm{Ca}\,T)^{-1}\left(1+h_{o\xi}^2\right)^{1/2} \times \left[2\left(1+h_{o\xi}^2\right)h_o^{-1}\psi_{\xi\eta} - 2h_{o\xi}\psi_{\xi\xi}\right. \\
&\quad \left. - 2\left(1+h_{o\xi}^2 - h_{o\xi\xi}h_o\right)h_o^{-2}h_{o\xi}\psi_\eta + \left(1+h_{o\xi}^2\right)(\tilde{p}+K_0)\right] - h_{o\xi\xi}, \\
N(\xi) &= -\mathrm{Ca}(1-\mathrm{Ca}\,T)^{-1}\left(1+h_{o\xi}^2\right)^{3/2}.
\end{aligned}$$

The form of conditions (16b)–(16d) assumes that h_o satisfies contact conditions (4) and volume constraint (3). Generalization to the case of time-dependent contact conditions and the (prescribed) variable volume constraint can easily be carried out. In the calculations, h_o is taken to be the shape of the interface from the previous outer iteration (or shape of the interface from the previous time step for the first outer iteration). For a sufficiently small time step a good approximation h_o of the interface is always available and this permits taking full advantage of the quadratic rate of convergence of the iterative process based on linearization (16). Typically, one or two iterations would reduce the error to several orders of magnitude less than the error accepted in the solution of the inner problem (see Section 3.3.1).

During each of the above iterations one has to solve problem (16). This is a linear problem; thus, its solution consists of a superposition of two linearly independent solutions and a particular solution of the inhomogeneous problem. Two boundary conditions (16b)–(16c) and volumetric constraint (16d) provide the required three conditions for determination of the two constants of superposition and the pressure constant K_1.

Problem (16) is solved directly. Equation (16a) is discretized using standard central-difference formulas and (16d) is approximated using the trapezoidal rule. The grid already used for determination of the flow field is used in both cases. The structure of the resulting matrix for the fixed contact point conditions, as well as for the fixed contact angle conditions, together with the optimized matrix inversion algorithm, are described in [2].

Numerical solution of (16) is very efficient and the required computing time is negligible, compared with the time required to determine solution of the inner problem (i.e., to determine the flow field).

An alternative version of the algorithm, following Ref. [2], has also been worked out. The normal stress condition (6i) is first discretized, resulting in a set of nonlinear algebraic equations. These equations are then linearized using the Newton–Raphson procedure. The resulting matrix has the same structure as the one resulting from the discretization of (16) and can be solved using the same matrix inversion algorithm. The algorithm based on Eqs. (16) was found to be about 20% more efficient computationally.

3.3.2.3. *Evaluation of the streamfunction at the interface.* The kinematic condition (6h) is written for time $t = (n+1)\Delta t$ and the time derivative h_t^{n+1} is replaced by backward, first-order finite-difference approximation, i.e.,

$$\left(\psi_\xi^{n+1}\right)_b = -(h^{n+1} - h^n)/\Delta t + O(\Delta t), \tag{17a}$$

where h^n stands for the known location of the interface at time $t = n\Delta t$ and h^{n+1} denotes the most recent approximation of h at time $t = (n+1)\Delta t$. The above formula is integrated to give

$$\psi_b^{n+1} = \left(\int_{-1/2L}^{\xi} h^n \, d\xi - \int_{-1/2L}^{\xi} h^{n+1} \, d\xi \right) \Bigg/ \Delta t \tag{17b}$$

and the integrals are evaluated using the trapezoidal rule. Equation (17b) shows that $\psi_b^{n+1}(-1/2L) = 0$, due to selection of the lower limit of integration, and $\psi_b^{n+1}(1/2L) = 0$, in view of (3).

Solution of the inner problem requires knowledge of ψ_b^{n+1}, $\left(\psi_\xi^{n+1}\right)_b$, and $(\psi_{\xi\xi}^{n+1})_b$; ψ_b^{n+1} is given by (17b), $(\psi_\xi^{n+1})_b$ is given by (17a), and $(\psi_{\xi\xi}^{n+1})_b$ is evaluated using the derivative of the kinematic condition $(\psi_{\xi\xi}^{n+1})_b = -h_{\xi t}^{n+1}$, where $h_{\xi t}^{n+1}$ is evaluated using finite-difference approximation similar to (14).

3.3.2.4. *Outer iterations.* A complete iterative cycle consists of determination of the flow field (inner problem) followed by determination of the new approximation for h^{n+1} and ψ_b^{n+1} (outer problem). Such (outer) iterations are carried out until the convergence criteria $|h_{i+1}^{n+1} - h_i^{n+1}| < \varepsilon_2$ and $|\mathrm{Res}_i| < \varepsilon_2$ are satisfied at all grid points along the interface. In the above, subscripts i, $i+1$ denote (outer) iteration numbers and Res stands for residuum of the normal stress condition. Calculations were typically carried out with $\varepsilon_2 = 10^{-6}$ and required 200–400 outer iterations per time step. The h_{i+1}^{n+1} was underrelaxed with the relaxation factor being a strong function of the capillary number Ca and decreasing from 1.0 to 0.001 with Ca increasing from 10^{-2} to O(1). The reader may recall that Ca is a measure of flexibility of the interface, with the higher values of Ca corresponding to the "softer" interface.

3.3.3. *Performance of the Algorithm*

The algorithm is self-starting and is formally second-order accurate in space and first-order accurate in time. The second-order spatial accuracy was numerically tested by Chen and Floryan [2] in the case of a steady algorithm. Since a very similar spatial discretization method was used in the unsteady algorithm described here, only spot checks for spatial accuracy have been carried out. These checks confirm that, indeed, the numerical results display error variation proportional to $\Delta\eta^2$ and $\Delta\xi^2$, even for interface deformation reaching 80% of the initial depth of the cavity. The questions of grid size selection and absolute error are discussed in Section 3.3.3.2.

Extensive tests have been carried out in order to verify the temporal accuracy. The calculations have been repeated with different time steps Δt and the tendency of the results as Δt decreased was observed. If one assumes that the discretization error can be expressed as $c(\Delta t)^\alpha$, with c being a constant (which is correct for the finite-difference approximation used here and for a sufficiently small time step Δt), the exponent α can be evaluated from the following relation:

$$\frac{\varepsilon_{2/3}}{\varepsilon_{1/2}} = \frac{(\Delta t_3)^\alpha - (\Delta t_2)^\alpha}{(\Delta t_2)^\alpha - (\Delta t_1)^\alpha}. \tag{18}$$

In the above, Δt_1, Δt_2, Δt_3 are different time steps used in the calculations, and $\varepsilon_{1/2}$ and $\varepsilon_{2/3}$ are distances between solutions obtained using time steps (Δt_1, Δt_2) and (Δt_2, Δt_3), respectively, expressed in terms of a suitable norm. In the present study, a root mean square norm was used; i.e.,

$$\varepsilon_{2/3} = \frac{1}{N}\sum_{i=1}^{N}\left[\left(S_3^n - S_2^n\right)^2\right]^{1/2}, \quad \varepsilon_{1/2} = \frac{1}{N}\sum_{i=1}^{N}\left[\left(S_2^n - S_1^n\right)^2\right]^{1/2}, \tag{19}$$

where S stands for a solution quantity, subscripts 1, 2, 3 refer to solutions obtained with time steps Δt_1, Δt_2, Δt_3, respectively, and summation extends over N suitably selected grid points. Quantities S are evaluated at the same instant of time using the same, sufficiently refined, spatial grid. In the present study, summations have been carried out over all internal grid points.

If $\Delta t_2 = 2\Delta t_1$, $\Delta t_3 = 2\Delta t_2$, Eq. (18) can be solved for α, i.e.,

$$\alpha = \ln(\varepsilon_{2/3}/\varepsilon_{1/2})/\ln(2). \tag{20}$$

Since the algorithm is first-order accurate in time, the expected value of the exponent is $\alpha = 1$. Departures from this value can be used as a measure of the loss of accuracy of the algorithm.

3.3.3.1. *Moving boundary problem.* The first test involves a moving boundary problem, i.e., the motion of the interface $h(\xi, t)$ is prescribed. In this case it is not necessary to solve for the interface deformation (Section 3.3.2.2). The value of the streamfunction at the interface at the next time step is given directly by the kinematic condition (6h) and it can be evaluated either analytically or numerically using (17), depending on the form of specification of $h(\xi, t)$. The solution process involves advancing the interface by a distance corresponding to Δt, followed by evaluation of the flow field corresponding to the new location of the interface, and so on.

Table I displays results of a test carried out for $L = 6$, $\mathrm{Re} = \mathrm{Ma} = 10$, $\mathrm{Bi} = 10^4$, $T_g(\xi, t) = -\xi$, fixed contact points condition, an initially flat interface, and a motionless liquid. Motion of the interface in the form

$$h(\xi, t) = 1 + \left(0.2\sin\left(\frac{2\pi\xi}{L}\right)\cdot\sin(\pi t)\right) \tag{21}$$

was imposed for $t = 0^+$. Calculations were carried out up to $t = 0.4$ (when maximum deformation was about 19%) with $\Delta t_1 = 1/20$, $\Delta t_2 = 1/10$, $\Delta t_3 = 1/5$, and $\Delta\xi = \Delta\eta = 1/20$. Results shown in Table I (Test 1) confirm the approximately first-order temporal accuracy of the algorithm. The reader may note that the vorticity is singular at the contact points and, thus, a small reduction in the expected value of $\alpha = 1$ should not be surprising. It took approximately 1088 (flow field) iterations per time step Δt_1, 1175 per time step Δt_2, and 1550 per time step Δt_3 with $\varepsilon_1 = 10^{-7}$.

TABLE I
Computed Values of the Exponent α (Eq. (20)) Describing the Temporal Accuracy

	Time	ψ	ω	T	p	h
Test 1	0.4	0.98	0.92	0.94	Not calculated	Not calculated
Test 2	0.8	0.94	0.88	0.93	1.07	1.05
	1.6	0.89	0.76	0.91	1.06	1.03
	2.2	0.83	0.70	0.90	1.05	1.02
Test 3	0.4	1.97	1.87	1.92	Not calculated	Not calculated
Test 4	0.4	1.8	1.31	1.60	0.98	1.05
	0.8	1.63	1.2	1.53	1.00	1.04
	1.6	1.05	0.82	1.02	1.02	1.03
	2.2	0.85	0.77	0.92	1.05	1.03
Test 5	0.8	1.94	1.79	1.81	2.07	2.01
	1.6	1.76	1.68	1.78	1.96	1.72
	2.2	1.70	1.63	1.75	1.86	1.67

Note. Test 1: moving boundary problem, one-step implicit method (for details see Section 3.3.3.1.); Test 2: free boundary problem, one-step implicit method (for details see Section 3.3.3.2); Test 3: moving boundary problem, two-step implicit method (for details see Section 3.6); Test 4: free boundary problem, two-step implicit method, mixed derivative $\psi_{\eta t}$ evaluated using Eq. (32) (for details see Section 3.6); Test 5: same as Test 4, mixed derivative $\psi_{\eta t}$ evaluated using Eq. (33).

3.3.3.2. *Free boundary problem.* The second test involves the complete problem; i.e., the shape of the interface results from the overall dynamics of the liquid and must be calculated. The interface was initially flat and the liquid was isothermal and motionless. The external heating in the form $T_g(\xi, t) = -\xi$ was imposed instantaneously at $t = 0^+$. The value of the capillary number was set to be 0.1 and the remaining test conditions were selected to be the same as in the previous section. No numerical instability problems have been encountered in all tests that have been carried out.

Figure 6 illustrates the effects of variation of the grid size on the accuracy of the results at locations where computations are very sensitive to grid refinement. These results show that grid size $\Delta\xi = \Delta\eta = 1/20$ provides satisfactory accuracy.

The values of exponent α describing temporal accuracy at $t = 0.8$, 1.6, and 2.2, when the maximum interface deformation reaches approximately 7%, 15.5%, and 21%, respectively, are given in Table I (Test 2). It can be seen that the algorithm maintains approximately first-order accuracy at all times. Figure 7 illustrates variations of the absolute error as a function of Δt at the same test points as in Fig. 6. It can be seen that $\Delta t = 0.1$ provides sufficient accuracy.

The timing information is based on calculations carried from $t = 0.2$ to $t = 0.8$ with $\varepsilon_1 = 10^{-7}$, $\varepsilon_2 = 10^{-6}$. The algorithm required on average 122 inner iterations per one outer iteration, and 420 outer iterations per one time step Δt_1. Similar numbers for Δt_2 were 230 and 338, and for Δt_3, 252 and 322. Overall, solution of the free boundary problem required about 10 times more computing time than solution of the moving boundary problem.

Examples of evolution of a flow system consisting of an initially quiescent isothermal liquid with a flat interface that is subject to an impulsive heating in the form $T_g(\xi) = -\xi$ imposed at time $t = 0^+$ are shown in Fig. 8 for the case of fixed contact points (Eq. (4a)) and

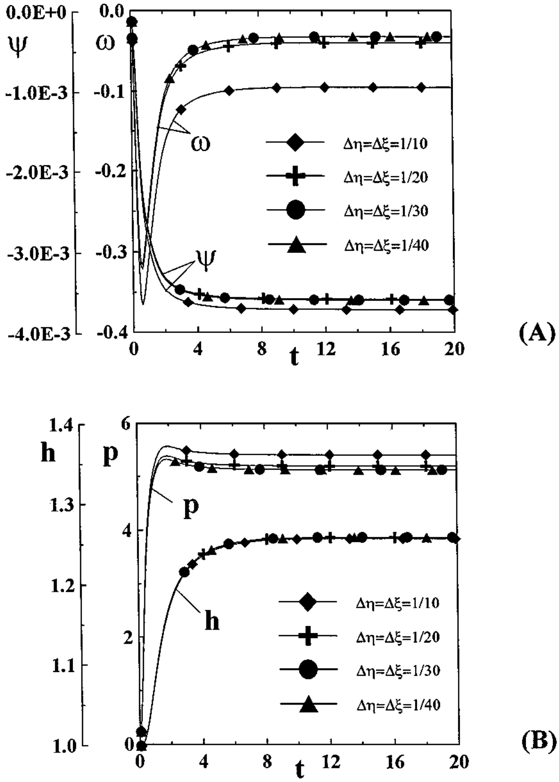

FIG. 6. Variation of ω and ψ at $(\xi, \eta) = (2.9, 0.9)$ (A) and h at $\xi = 1.5$ and p at $\xi = 2.9$ (B) as a function of grid size $\Delta\xi$, $\Delta\eta$. Test conditions are described in Section 3.3.3.2. $\Delta t = 0.1$ in all calculations.

in Fig. 9 for the case of fixed contact angles (Eq. (4b)) with $\theta_L = \theta_R = 0$. The reader may note a very strong effect of the type of contact conditions on the evolution of the flow system.

As an additional test, the case of transition from steady to oscillatory convection reported in Ref. [9] for $L = 2$, $\mathrm{Re} = 220$, $\mathrm{Ma} = 2.2$ has been investigated. Results obtained using the present algorithm are in agreement with those described in [9].

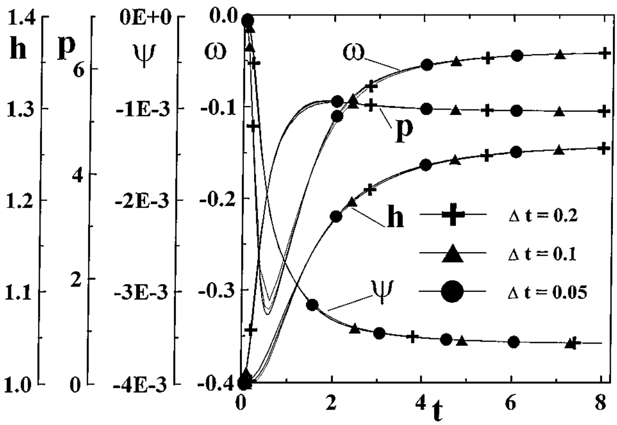

FIG. 7. Variation of ω and ψ at $(\xi, \eta) = (2.9, 0.9)$ and h at $\xi = 1.5$ and p at $\xi = 2.9$ as a function of Δt. Other test conditions as in Fig. 6. $\Delta\xi = \Delta\eta = 1/20$ in all calculations.

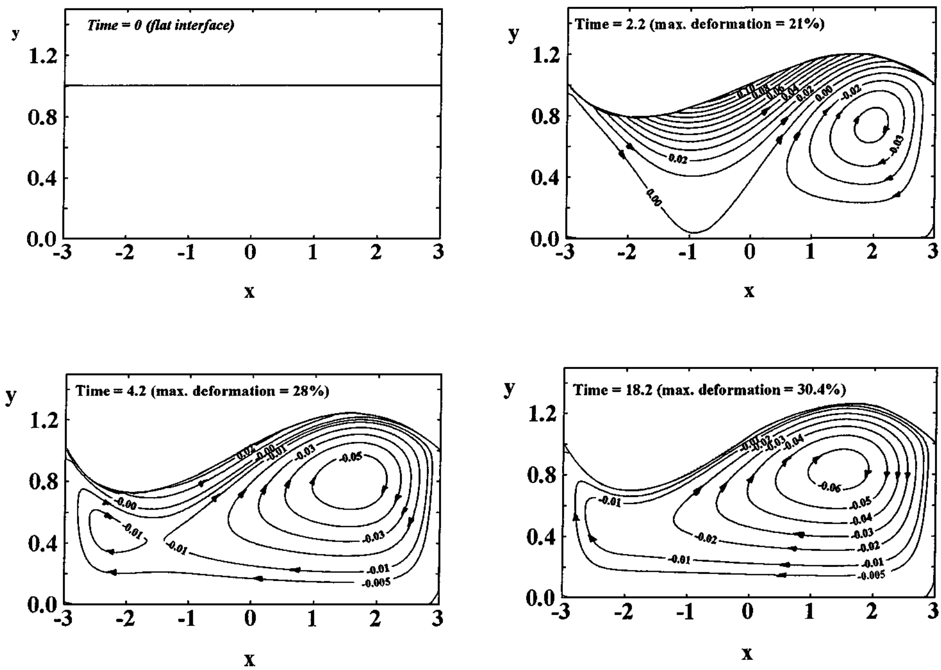

FIG. 8. Flow patterns resulting from an impulsive heating in the form $T_g(\xi) = -\xi$ imposed at time $t = 0^+$. Fixed contact points case (Eq. (4a)). Calculations carried out with $\Delta\xi = \Delta\eta = 1/20$ and $\Delta t = 0.2$. Last picture corresponds to steady-state flow pattern.

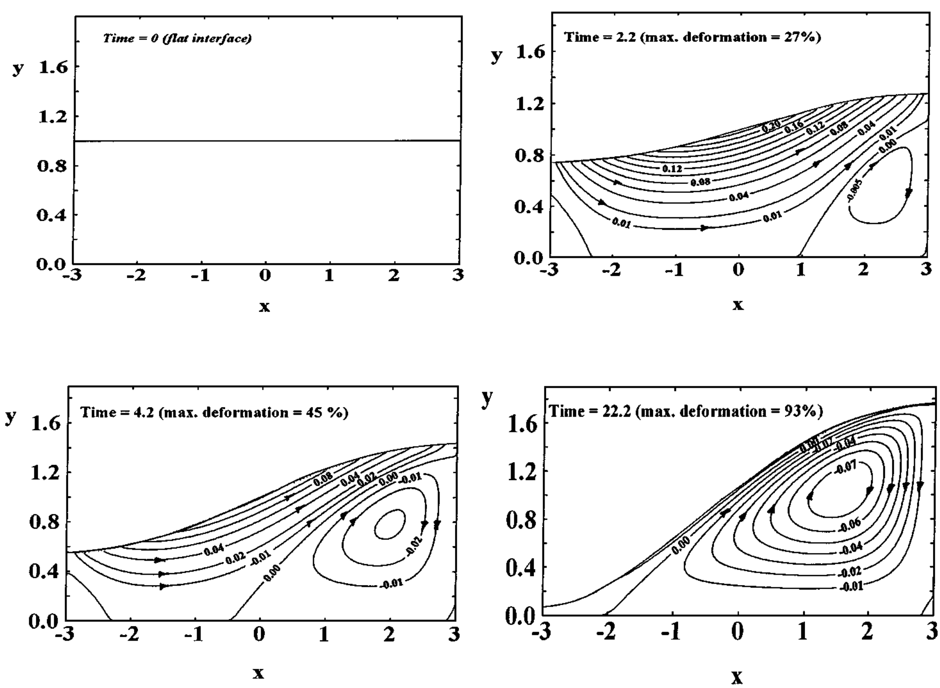

FIG. 9. Flow patterns resulting from an impulsive heating in the form $T_g(\xi) = -\xi$ imposed at time $t = 0^+$. Fixed contact angles case (Eq. (4b)). Calculations carried out with $\Delta\xi = \Delta\eta = 1/20$ and $\Delta t = 0.2$. No steady state has been reached.

3.4. The Crank–Nicolson Method

A relatively high computational cost of the one-step implicit method motivates search for a faster algorithm. The Crank–Nicolson method is formally second-order accurate in time; thus it permits use of larger time steps while maintaining the same absolute accuracy.

We assume that all quantities at time $t = n\Delta t$ are known and seek their values at time $t = (n+1)\Delta t$. The logical structure of the algorithm is the same as already described in Section 3.3. The following description is limited only to those elements of the algorithm that are different from the one-step implicit method.

The vorticity transport equation is written at time $t = (n+1/2)\Delta t$ in the form

$$\begin{aligned}\frac{\omega^{n+1}-\omega^n}{\Delta t} &+ (h^{n+1/2})^{-1}\left(\psi_\eta^{n+1/2}\cdot\omega_\xi^{n+1/2} - \psi_\xi^{n+1/2}\cdot\omega_\eta^{n+1/2}\right)\\ &+ \eta(h^{n+1/2})^{-1}\omega_\eta^{n+1/2}\left(\psi_\xi^{n+1/2}\right)_b - \nabla^2\omega^{n+1/2}/\mathrm{Re} = 0,\end{aligned} \tag{22}$$

where $\omega_t^{n+1/2}$ has been replaced by central, second-order finite-difference approximation, $h_t^{n+1/2}$ was replaced by $(\psi_\xi^{n+1/2})_b$ by taking advantage of the kinematic condition (6h), and superscripts n, $(n+1/2)$, $(n+1)$ refer to time steps $t = n\Delta t$, $t = (n+1/2)\Delta t$, $t = (n+1)\Delta t$, respectively. All terms written at time $(n+1/2)\Delta t$ are then expressed in terms of their values at $n\Delta t$ and $(n+1)\Delta t$, using linear interpolation, e.g., $\omega_\xi^{n+1/2} = 1/2(\omega_\xi^n + \omega_\xi^{n+1})$, etc. The energy transport equation has the same form as (22) with ω replaced by T and Re replaced by Ma. The streamfunction at time $t = (n+1)\Delta t$ is computed from (7a).

The spatial derivatives are discretized using the grid and the finite-difference approximations already described in Section 3.3.1. The discretized form of (22) can be easily derived and is omitted from this presentation. The solution to the outer problem has the same logical structure as described in Section 3.3.2. Pressure is evaluated by writing Eq. (11a) at time $t = (n+1/2)\Delta t$ and approximating the mixed derivatives $\psi_{\eta t}^{n+1/2}$, $\psi_{\xi t}^{n+1/2}$ as

$$\begin{aligned}(\psi_{\xi t})_0 &= \left[\psi_2^{n+1} - \psi_2^n - \psi_1^{n+1} + \psi_1^n\right]/(2\Delta\xi\,\Delta t) + O(\Delta t^2) + O(\Delta\xi^2),\\ (\psi_{\eta t})_0 &= \left[3\left(\psi_0^{n+1} - \psi_0^n\right) - 4\left(\psi_1^{n+1} - \psi_1^n\right) + \psi_2^{n+1} - \psi_2^n\right]/(2\Delta\eta\Delta t)\\ &\quad + O(\Delta t^2) + O(\Delta\eta^2),\end{aligned} \tag{23}$$

where subscripts refer to grid points shown in Fig. 10. The remaining quantities in (11a) are expressed in terms of their values at $t = n\Delta t$ and $t = (n+1)\Delta t$ using linear interpolation. The resulting equation is then solved for p_ξ^{n+1} and subsequently integrated to get p^{n+1}. Details of this process are omitted. One may note that p^{n+1} depends explicitly on p^n.

The new location of the interface is evaluated using the method described in Section 3.3.2.2. The value of the streamfunction at the interface is evaluated by writing the kinematic condition (6h) at time $t = (n+1/2)\Delta t$, replacing the time derivative $h_t^{n+1/2}$ by central, second-order finite-difference approximation and expressing $(\psi_\xi^{n+1/2})_b$ in terms of $(\psi_\xi^n)_b$ and $(\psi_\xi^{n+1})_b$ using linear interpolation. The resulting equation is solved for $(\psi_\xi^{n+1})_b$ and integrated, resulting in

$$(\psi^{n+1})_b = -\psi_b^n - 2\left(\int_{-1/2L}^{\xi} h^{n+1}\,d\xi - \int_{-1/2L}^{\xi} h^n\,d\xi\right)\Big/\Delta t \tag{24}$$

and the integrals are evaluated using the trapezoidal rule.

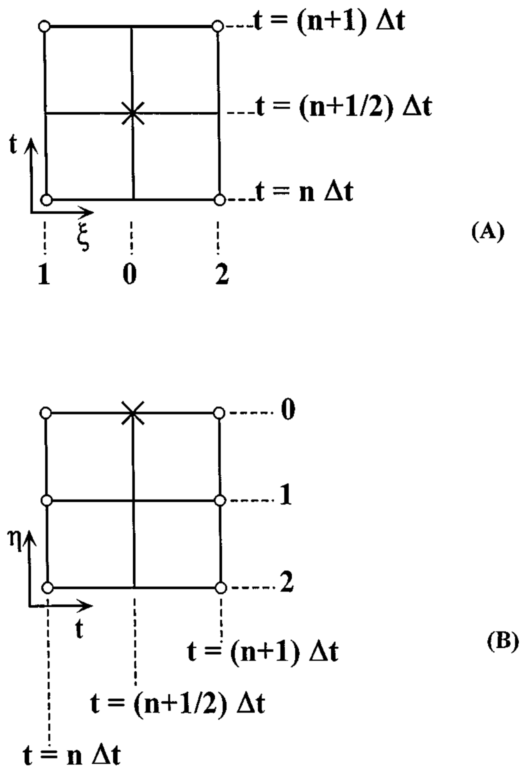

FIG. 10. Sketch of a computational module used to evaluate $\psi_{\xi t}^{n+1/2}$ (A) and $\psi_{\eta t}^{n+1/2}$ (B) at the interface in the Crank–Nicolson method.

The algorithm requires knowledge of the flow at only one time step in order to predict the motion of the liquid at the next time step. The algorithm is in principle self-starting. Correct results will be obtained, however, only if a consistent set of initial conditions is available, including the flow field, the shape of the interface, and ψ_ξ (or h_t). The determination of such conditions is in practice nearly impossible. The algorithm may produce very inaccurate (even wrong) results when inconsistent data are used. This can be seen, for example, in Eq. (24) which requires values of ψ_b at $n=0$ in order to predict ψ_b at $n=1$. The above conclusion has been confirmed by various tests involving grid convergence studies and comparisons with results obtained using other methods described in this paper. It is recommended, therefore, that when no good initial data is available the Crank–Nicolson algorithm should not be used for the first time step. In all calculations reported here the one-step implicit method was used to start the calculations.

The algorithm is formally second-order accurate in time and space and, thus, it could potentially significantly reduce the cost of calculations. Unfortunately, the temporal accuracy gains are offset by numerical instability problems which dictate the use of very small time steps.

The numerical instabilities will be illustrated in the context of the test problem already introduced in Section 3.3.3.2, i.e., $L=6$, $\mathrm{Re}=\mathrm{Ma}=10$, $\mathrm{Ca}=0.1$, $\mathrm{Bi}=10^4$, the fixed contact points condition, an initially flat interface, and a motionless liquid subject to an instantaneous heating $T_g(\xi,t)=-\xi$ imposed at $t=0^+$, $\Delta\xi=\Delta\eta=1/20$, $\Delta t=0.2$.

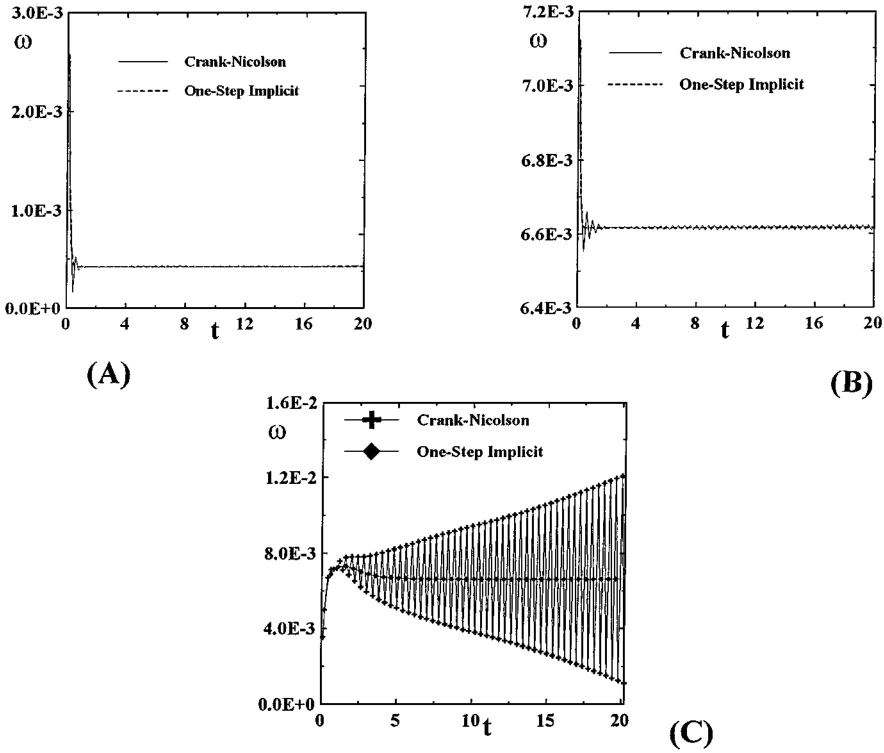

FIG. 11. Variations of vorticity as a function of time at $(\xi, \eta) = (-3, 0.1)$ obtained using the Crank–Nicolson method with $\Delta\xi = \Delta\eta = 1/20$, $\Delta t = 0.2$: (A) flat nondeformable interface; (B) curved nondeformable interface; (C) complete free boundary problem. Other details of the tests are described in Section 3.4. Results obtained using the one-step implicit method are shown for reference purposes.

Figure 11A illustrates computed values of ω as a function of time at a test point $\xi = -3$, $\eta = 0.1$ for a reference fixed boundary problem in which the interface is flat and does not deform. The reader may note the appearance of a numerical instability at the very beginning of the calculations which is due to discontinuity of the initial conditions. The algorithm damps out this instability and the results for $t > 1$ obtained using the Crank–Nicolson method overlap with those obtained using the one-step implicit method.

Figure 11B illustrates the behaviour of the algorithm for a curved, but fixed, interface. The shape of the interface used in the calculations was obtained by solving the complete problem for $t \to \infty$ using the one-step implicit method. It can be seen that the numerical instability triggered by the discontinuity in the initial conditions is somewhat larger (than for the flat interface) but the algorithm is able to damp it out. A very weak instability appears for $t > 3$ when the solution reaches the steady-state limit. This instability is very benign and does not prevent generation of useful results.

Figure 11C illustrates the behaviour of the algorithm for the complete problem where the location of the interface has to be calculated. The occurrence of a very strong numerical instability is clearly visible. This instability is associated with the motion of the interface, as documented by the tests discussed above.

A series of tests has been carried out in order to assess the effect of the presence of discontinuity in the initial conditions on the numerical instability. The heating was assumed

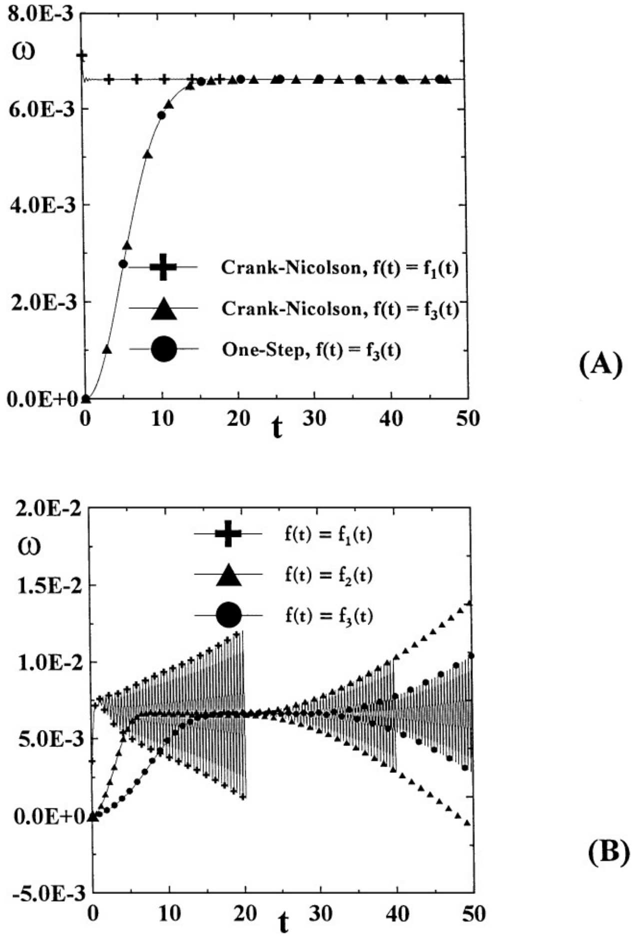

FIG. 12. Variations of vorticity as a function of time at $(\xi, \eta) = (-3, 0.1)$ obtained using the Crank–Nicolson method with $\Delta\xi = \Delta\eta = 1/20$, $\Delta t = 0.2$ for different rates of heating: (A) curved nondeformable interface, results obtained using the one-step implicit method are shown for reference purposes; (B) complete free boundary problem. Functions $f_1(t)$, $f_2(t)$, $f_3(t)$ describe different rates of heating (see Eq. (25)). Other details of the tests are described in Section 3.4.

in the form

$$T_g(\xi, t) = -\xi \cdot f_i(t), \quad i = 1, 2, 3, \tag{25}$$

where $f_1(t) = \mathrm{H}(t)$, $f_2(t) = 1 - \exp(-0.1t^2)$, $f_3(t) = 1 - \exp(-0.02t^2)$, and $\mathrm{H}(t)$ denotes the Heaviside function. The reader may note that the rate of heating is reduced by replacing $f_1(t)$ with $f_2(t)$, and $f_2(t)$ with $f_3(t)$. Figure 12A, displaying results for the case of deformed but fixed interface (as in Fig. 11B), shows that the reduction in the strength of the discontinuity in the initial conditions eliminates the instability. Figure 12B, displaying results of the complete problem, shows that the reduction of the initial discontinuity delays the onset of the instability, but does not eliminate it. It can be concluded that the instability is not triggered by the initial discontinuity but is an intrinsic property of the algorithm.

Figure 13A shows the effect of reduction of the grid size on the instability, while Fig. 13B shows the effect of reduction of the temporal step size. It can be concluded, on the basis of

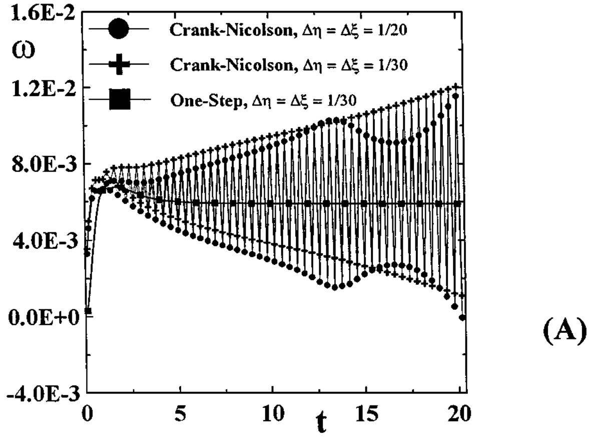

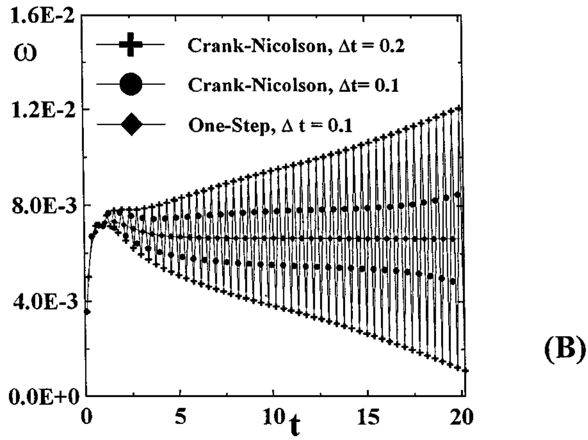

FIG. 13. Variations of vorticity as a function of time at $(\xi, \eta) = (-3, 0.1)$ for the complete free boundary problem obtained using the Crank–Nicolson method: (A) effects of changing the spatial grid size $\Delta\xi$, $\Delta\eta$ with $\Delta t = 0.2$; (B) effects of changing step size Δt with $\Delta\xi = \Delta\eta = 1/20$. Other details of the tests are described in Section 3.4. Results obtained using the one-step implicit method are shown for reference purposes.

these results, that the algorithm is most likely to be conditionally stable. While no attempt has been made to determine the critical stability conditions, the results shown in Fig. 13 suggest that very small step sizes $\Delta\xi$, $\Delta\eta$, Δt might be required in order to stabilize the calculations. Under such conditions, the Crank–Nicolson algorithm will be more expensive computationally than the one-step implicit algorithm.

The final test deals with the moving boundary problem that has already been introduced in Section 3.3.3.1. In this problem the motion of the interface is prescribed by Eq. (21). Results obtained at $\Delta\xi = \Delta\eta = 1/20$ and $\Delta t = 0.2$ shown in Fig. 14 demonstrate the occurrence of a numerical instability very similar to the one described above, even in this (much simpler) problem. The strength of the instability appears to be similar for both (the free and the moving) boundary problems.

3.5. The Trapezoidal Method

Numerical stability problems encountered in the Crank–Nicolson method make this method impractical due to the high computational cost. The present section is devoted

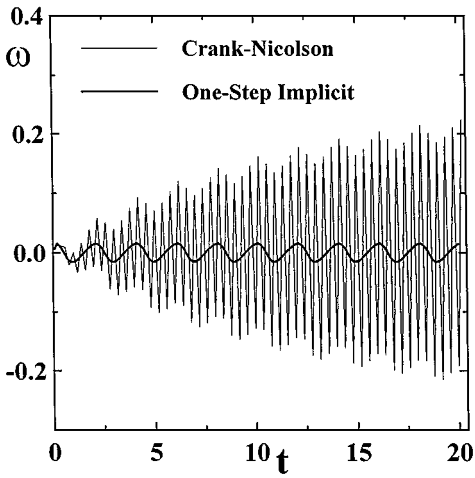

FIG. 14. Variations of vorticity as a function of time at $(\xi, \eta) = (-3, 0.1)$ for the moving boundary problem with the motion of the interface prescribed by Eq. (21) obtained using the Crank–Nicolson method with $\Delta\xi = \Delta\eta = 1/20$, $\Delta t = 0.2$. Other details of the tests are described in Section 3.4. Results obtained using the one-step implicit method are shown for reference purposes.

to an alternative algorithm that is also second-order accurate in time and also relies on information from just one previous time step, i.e., the trapezoidal method.

The vorticity transport equation is integrated from $t = n\Delta t$ to $t = (n+1)\Delta t$ using the trapezoidal rule and rearranged into the form

$$\omega^{n+1} - \frac{\Delta t}{2} G^{n+1} = \omega^n + \frac{\Delta t}{2} G^n, \tag{26}$$

where $G = -h^{-1}(\psi_\eta \omega_\xi - \psi_\xi \omega_\eta) - \eta h^{-1} \omega_\eta (\psi_\xi)_b + \nabla^2 \omega/\mathrm{Re}$, h_t was replaced by $(\psi_\xi)_b$, superscripts $n, n+1$ refer to time steps, and subscript b denotes the value of the field variable determined at the interface. The energy equation is integrated in a similar fashion. The streamfunction at time $t = (n+1)\Delta t$ is computed from (7a).

Determination of the shape of the interface at time $t = (n+1)\Delta t$ hinges on prior evaluation of the pressure at that time. Use of Eq. (11) reduces the temporal accuracy to first-order because of the presence of mixed derivatives. Second-order accuracy can be maintained, provided that values of various interfacial quantities for $t = (n-1)\Delta t$ and $t = n\Delta t$ are available. Since our objective is to develop an algorithm that relies on information available at only one previous time step, a completely different method for pressure evaluation has to be found.

Equation (1b) is integrated between $t = n\Delta t$ and $t = (n+1)\Delta t$ using the trapezoidal rule and expressed in the (ξ, η) plane using the streamfunction and vorticity. Equation (1c) is multiplied by h_ξ, integrated between $t = n\Delta t$ and $t = (n+1)\Delta t$ using a combination of integration by parts and the trapezoidal rule and making use of kinematic condition (6h). The resulting two equations are combined and simplified using (6a) to give the expression

$$p_\xi^{n+1} = -p_\xi^n + (Z_1 + Z_2)^{n+1} + (Z_1 + Z_2)^n + Z_3^{n+1} - Z_3^n, \tag{27}$$

where

$$
\begin{aligned}
Z_1 &= \omega_\xi h_\xi, \\
Z_2 &= -h^{-1}\left(1+h_\xi^2\right)\omega_\eta + Re\,\psi_\xi[-\omega + h^{-1}h_\xi\psi_{\xi\eta}] + \mathrm{Re}\,h^{-1}\psi_\eta\left[-h^{-1}\left(1+h_\xi^2\right)\psi_{\xi\eta}\right. \\
&\quad \left. + \left(h_{\xi\xi} - h^{-1}h_\xi^2\right)\psi_\xi - h^{-2}h_\xi\left(-h_\xi^2 + hh_{\xi\xi} - 1\right)\psi_\eta\right], \\
Z_3 &= 2\mathrm{Re}\,(\Delta t)^{-1}\left[h_\xi\psi_\xi - h^{-1}\left(1+h_\xi^2\right)\psi_\eta\right].
\end{aligned}
$$

In the above, subscripts n and $n+1$ refer to time steps. Equation (27) is integrated between $\xi = 0$ and $\xi = a$ to get $\tilde{p}^{n+1}$; i.e.,

$$
\begin{aligned}
\tilde{p}^{n+1}(a) &= \tilde{p}^{n+1}(0) - \tilde{p}^n(a) + \tilde{p}^n(0) + \left[(\omega h_\xi)^{n+1} + (\omega h_\xi)^n\right]_{\xi=a} \\
&\quad - \left[(\omega h_\xi)^{n+1} + (\omega h_\xi)^n\right]_{\xi=0} - \left(\int_o^a \omega h_\xi\, d\xi\right)^{n+1} - \left(\int_o^a \omega h_\xi\, d\xi\right)^{n} \\
&\quad + \int_o^a \left(Z_2^{n+1} + Z_2^n\right) d\xi + \int_o^a \left(Z_3^{n+1} - Z_3^n\right) d\xi + K^{n+1}.
\end{aligned}
\tag{28}
$$

The remaining integrals are evaluated using the trapezoidal rule. One may note that (28) requires knowledge of the pressure at the previous time step. The new location of the interface is evaluated using the method described in Section 3.3.2.2. The value of the streamfunction at the interface is evaluated by integrating the kinematic condition (6h) between $t = n\Delta t$ and $t = (n+1)\Delta t$ using the trapezoidal rule and integrating with respect to ξ to get

$$
(\psi^{n+1})_b = -(\psi^n)_b - 2(\Delta t)^{-1}\int_{-1/2L}^{\xi} (h^{n+1} - h^n)\, d\xi, \tag{29}
$$

where the remaining integral is to be evaluated using the trapezoidal rule.

The algorithm requires knowledge of the flow at only one time step in order to predict the motion of the liquid at the next time step. While the algorithm is, in principle, self-starting, it requires a consistent set of initial conditions, as was the case with the Crank–Nicolson method (see Section 3.4). Because such conditions are rarely available, it is recommended that the trapezoidal method should not be used for the first time step. In all calculations reported here the one-step implicit method described in Section 3.3 was used to start the calculations.

The algorithm is second-order accurate in time but, unfortunately, suffers from numerical instabilities which dictate the use of rather small time steps. These instabilities are weaker than those found in the case of the Crank–Nicolson method, however.

The numerical instabilities will be described in the context of the same test problem as used to illustrate the Crank–Nicolson method (see Section 3.4) and with the same spatial and temporal grid resolutions, i.e., $\Delta\xi = \Delta\eta = 1/20$ and $\Delta t = 0.2$.

Figure 15A shows variations of ω as a function of time at a test point $\xi = -3$, $\eta = 0.1$ for a reference problem, where the interface is flat and fixed. An instability due to discontinuity of initial conditions can be observed. This instability is damped out for $t > 1$. Figure 15B illustrates the behaviour of the algorithm for a curved but fixed interface, whose shape was selected in the same way as in the case of the Crank–Nicolson method (Section 3.4). An

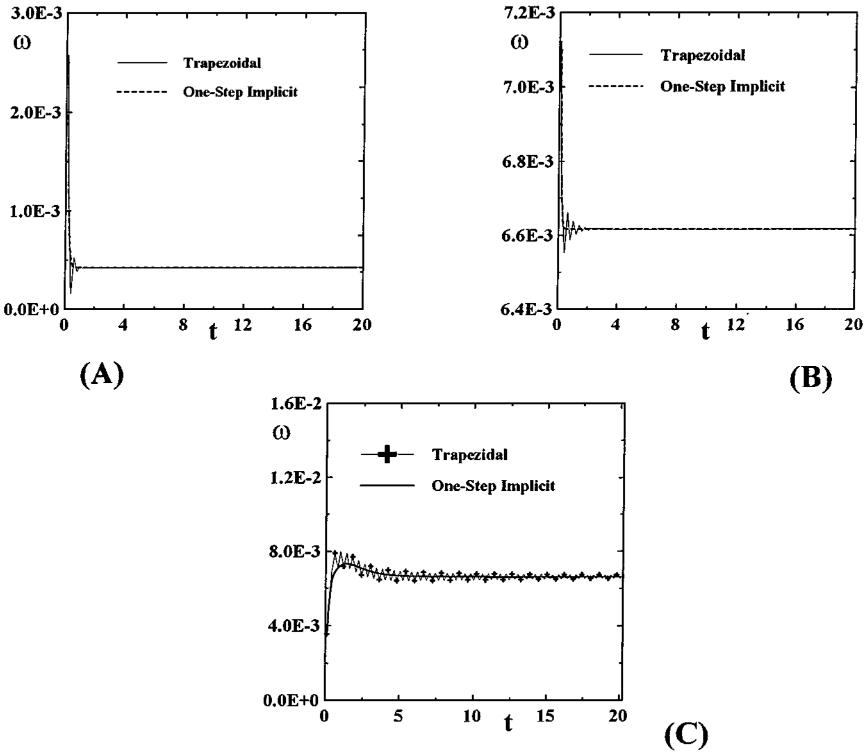

FIG. 15. Variations of vorticity as a function of time at $(\xi, \eta) = (-3, 0.1)$ obtained using the trapezoidal method with $\Delta\xi = \Delta\eta = 1/20$, $\Delta t = 0.2$: (A) flat nondeformable interface; (B) curved nondeformable interface; (C) complete free boundary problem. Other details of the tests are described in Section 3.5. Results obtained using the one-step implicit method are shown for reference purposes.

instability due to discontinuity in the initial conditions is quickly damped out and no new instability appears, unlike the case of the Crank–Nicolson method (see Fig. 11B). Figure 15C illustrates the behaviour of the algorithm for the full problem, where the location of the interface has to be calculated. The instability does occur, but it is much weaker than in the case of the Crank–Nicolson method (see Fig. 11C).

Figure 16 shows that smoothing out the discontinuity in the initial conditions through reduction in the rate of heating (see Eq. (25)) eliminates the instability. A very weak instability appears spontaneously for $t > 25$ when the solution reaches steady-state limit, but it does not prevent generation of useful results.

Figure 17 shows that the reduction of the spatial grid size has a very small effect on the instability, at least for the range of grids considered. Figure 18 demonstrated that the reduction of the time step Δt significantly reduces the instability. Figure 19 deals with the case of the motion of the interface prescribed by Eq. (21). No instability is detected, unlike the case of the Crank–Nicolson method (see Fig. 14).

It can be concluded, on the basis of the above tests, that the trapezoidal method is conditionally stable. No attempt has been made to determine the critical stability conditions. The available results show, nevertheless, that the grid and step sizes required to stabilize the method are too small to make it competitive with the one-step implicit method. The trapezoidal method is more stable than the Crank–Nicolson method and, unlike the Crank–Nicolson method, it can be used to solve the moving boundary problems (with the prescribed

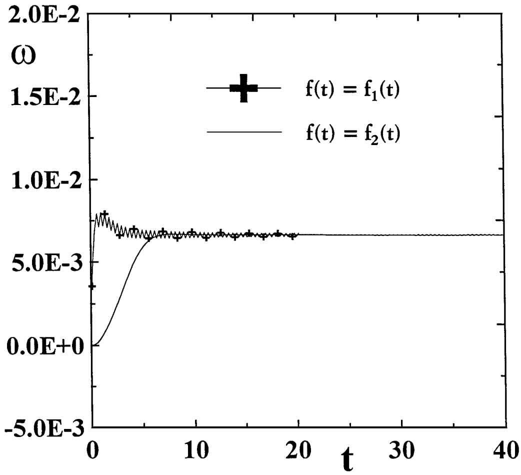

FIG. 16. Variations of vorticity as a function of time at $(\xi, \eta) = (-3, 0.1)$ obtained using the trapezoidal method with $\Delta\xi = \Delta\eta = 1/20$, $\Delta t = 0.2$ for different rates of heating for the complete free boundary problem. Functions $f_1(t)$, $f_2(t)$ describe different rates of heating (see Eq. (25)). Other details of the tests are described in Section 3.5.

motion of the interface). The instability occurs only for free boundary problems, where the location of the interface has to be calculated.

3.6. The Two-Step Implicit Method

The numerical instability problems identified in the case of the Crank–Nicolson and trapezoidal methods made them uncompetitive compared with the one-step implicit method. In this section we shall continue our search for a more computationally efficient (and stable) algorithm and consider a two-step implicit method.

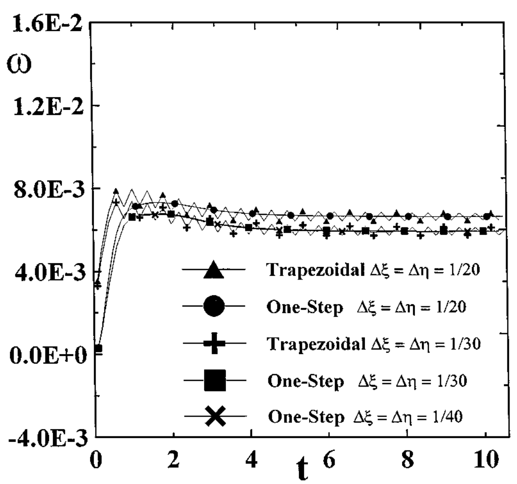

FIG. 17. Variations of vorticity as a function of time at $(\xi, \eta) = (-3, 0.1)$ obtained using the trapezoidal method for the complete free boundary problem with different step sizes $\Delta\xi$, $\Delta\eta$ and with $\Delta t = 0.2$. Other details of the tests are described in Section 3.5. Results obtained using the one-step implicit method are shown for reference purposes.

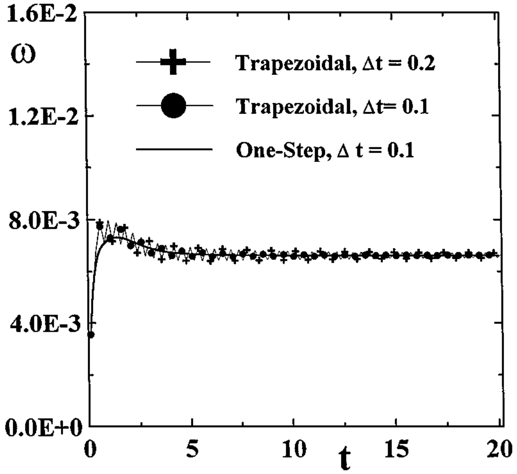

FIG. 18. Variations of vorticity as a function of time at $(\xi, \eta) = (-3, 0.1)$ obtained using the trapezoidal method for the complete free boundary problem with different step sizes Δt and with $\Delta\xi = \Delta\eta = 1/20$. Other details of the tests are described in Section 3.5. Results obtained using the one-step implicit method are shown for reference purposes.

In the further considerations, it is assumed that all flow quantities at times $t = (n-1)\Delta t$ and $t = n\Delta t$ are available. The logical structure of the algorithm is the same as already described in Section 3.3.

The vorticity transport equation is written at time $t = (n+1)\Delta t$ in the form

$$\frac{3\omega^{n+1} - 4\omega^n + \omega^{n-1}}{2\Delta t} + (h^{n+1})^{-1}\left(\psi_\eta^{n+1} \cdot \omega_\xi^{n+1} - \psi_\xi^{n+1} \cdot \omega_\eta^{n+1}\right)$$
$$+ \eta (h^{n+1})^{-1} \omega_\eta^{n+1} \left(\psi_\xi^{n+1}\right)_b - \nabla^2 \omega^{n+1}/\mathrm{Re} = 0, \tag{30}$$

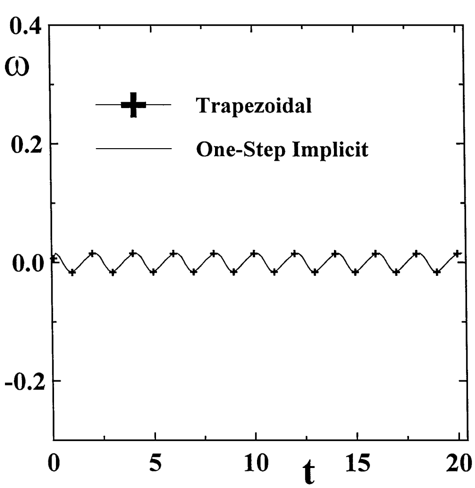

FIG. 19. Variations of vorticity as a function of time at $(\xi, \eta) = (-3, 0.1)$ obtained using the trapezoidal method for the moving boundary problem with the motion of the interface prescribed by Eq. (21) with $\Delta\xi = \Delta\eta = 1/20$, $\Delta t = 0.2$. Other details of the tests are described in Section 3.5. Results obtained using the one-step implicit method are shown for reference purposes.

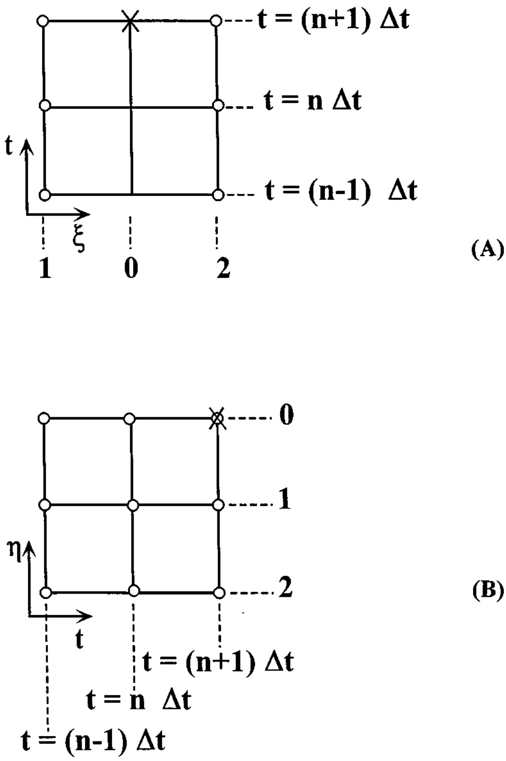

FIG. 20. Sketch of a computational module used to evaluate $\psi_{\xi t}$ (A) and $\psi_{\eta t}$ (B) at the interface in the two-step implicit method.

where ω^{n+1} has been replaced by backward, second-order finite-difference approximation, h_t^{n+1} was replaced by $(\psi_\xi^{n+1})_b$ using (6h), superscripts $n-1, n, n+1$ refer to time steps, b denotes the value of the field variable at the interface, and h^{n+1} is considered known. The energy equation has the same form as (30) with ω replaced by T, and Re replaced Ma. The streamfunction is computed from (7a).

The spatial derivatives are discretized using the grid and the finite-difference approximations already described in Section 3.3.1. The discretized form of (30) can be easily derived and is omitted from this presentation.

The magnitude of p_ξ^{n+1} is given by Eq. (11b). Spatial derivatives are evaluated as described in Section (3.3.2.1). Mixed derivative $\psi_{\xi t}$ has been evaluated using the formula

$$(\psi_{\xi t})_0 = \left[3\left(\psi_2^{n+1} - \psi_1^{n+1}\right) - 4\left(\psi_2^n - \psi_1^n\right) + \psi_2^{n-1} - \psi_1^{n-1}\right]/(4\Delta t\Delta\xi) + O(\Delta t^2) + O(\Delta\xi^2), \tag{31}$$

where subscripts refer to points shown in Fig. 20A. Two types of formulas were used for $\psi_{\eta t}$, i.e., either

$$(\psi_{\eta t})_0 = \left[7\psi_0^{n+1} + 8\left(\psi_1^n - \psi_1^{n+1} - \psi_0^n\right) - \psi_2^{n-1} + \psi_0^{n-1} + \psi_2^{n-1}\right]/(4\Delta t\Delta\eta) + O(\Delta t)^2 + O(\Delta t\cdot\Delta\eta) + O(\Delta\eta)^2 \tag{32}$$

or

$$(\psi_{\eta t})_0 = \left[3\left(3\psi_0^{n+1} - 4\psi_1^{n+1} + \psi_2^{n+1}\right) - 4\left(3\psi_0^n - 4\psi_1^n + \psi_2^n\right) + 3\psi_0^{n-1} - 4\psi_1^{n-1} + \psi_2^{n-1}\right]/(4\Delta t \Delta\eta) + O(\Delta t)^2 + O[(\Delta t)^2 \cdot (\Delta\eta)^2] + O(\Delta\eta)^2, \tag{33}$$

where subscripts refer to points shown in Fig. 20B. Expression (33) is preferred because it is second-order accurate in time. Equation (32), while being only first-order accurate in time, is nevertheless acceptable because the absolute error is $O(\Delta t, \Delta\eta)$ and, thus, sufficiently small for most applications. Integration of p_ξ^{n+1} is carried out as described in Section (3.3.2.1). The new location of the interface is evaluated using method described in Section 3.3.2.2. The streamfunction at the interface is evaluated by writing the kinematic condition (6h) at time $t = (n+1)\Delta t$ and replacing the time derivative h_t^{n+1} by backward, second-order, finite-difference approximation; i.e.,

$$\left(\psi_\xi^{n+1}\right)_b = -(3h^{n+1} - 4h^n + h^{n-1})/(2\Delta t) + O(\Delta t)^2, \tag{34}$$

where h^{n-1}, h^n denote the known locations of the interface at times $t = (n-1)\Delta t$, $t = n\Delta t$, respectively, and h^{n+1} denotes the most recent approximations of h at time $t = (n+1)\Delta t$. Integration of (34) gives

$$(\psi^{n+1})_b = \left(3\int_{-1/2L}^{\xi} h^{n+1}\, d\xi - 4\int_{-1/2L}^{\xi} h^n\, d\xi + \int_{-1/2L}^{\xi} h^{n-1}\, d\xi\right) \Big/ (2\Delta t), \tag{35}$$

where all integrals are evaluated using the trapezoidal rule.

Since the algorithm requires information from two previous time steps in order to predict the behaviour of the flow at the next time step, the algorithm is not self-starting. All results reported here have been obtained with the one-step implicit method used to initiate the calculations. No numerical instability problems have been encountered.

The algorithm is formally second-order accurate in space and time. The spatial accuracy was tested by Chen and Floryan [2] in the case of a steady algorithm. Since a very similar spatial discretization is used here, only spot checks for spatial accuracy have been carried out. These results do confirm that the error variation is proportional to $\Delta\eta^2$ and $\Delta\xi^2$ even for large interfacial deformations. The questions of grid size selection and absolute accuracy are discussed in the following paragraphs.

The first test involves the moving boundary problem introduced in Section 3.3.3.1. The reader may recall that the motion of the interface is prescribed by Eq. (21). Calculations were carried out from $t = 0$ to $t = 0.4$ with $\Delta t_1 = 1/20$, $\Delta t_2 = 1/10$, $\Delta t_3 = 1/5$, and $\Delta\xi = \Delta\eta = 1/20$. Results shown in Table I (Test 3) confirm the approximately second-order temporal accuracy of the algorithm. It took approximately 875 of (the flow field) iterations per time step Δt_1, 960 per time step Δt_2, and 1100 per time step Δt_3 with $\varepsilon_1 = 10^{-7}$.

The second test involves the complete problem introduced in Section 3.3.3.2. The reader may recall that the location of the interface has to be calculated as a part of the solution procedure. Eq. (33) is used to approximate $\psi_{\eta t}$ unless otherwise noted.

Figure 21 illustrates the effects of variations of grid size on the accuracy of the results at locations where computations are very sensitive to grid refinement. These results show that the grid size $\Delta\xi = \Delta\eta = 1/20$ provides sufficient accuracy.

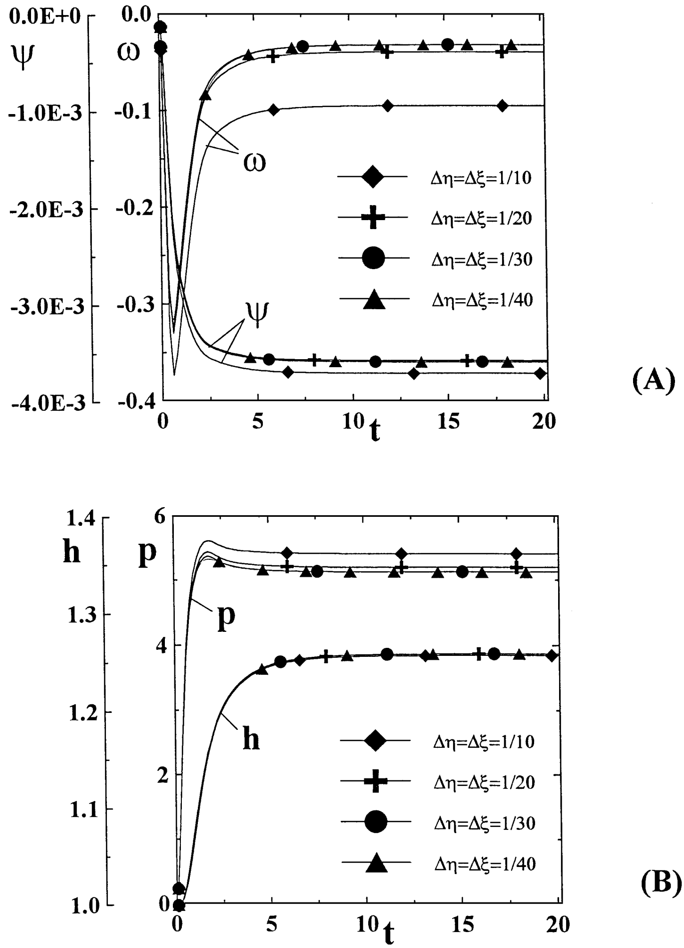

FIG. 21. Variation of ω and ψ at $(\xi, \eta) = (2.9, 0.9)$ (A) and h at $\xi = 1.5$ and p at $\xi = 2.9$ (B) as a function of grid size $\Delta\xi$, $\Delta\eta$. Test conditions are described in Section 3.6; $\Delta t = 0.2$ in all calculations.

Values of the exponent α describing temporal accuracy at $t = 0.8$, 1.6, 2.2, when the maximum interface deformation reaches approximately 7%, 15.5%, and 21%, respectively, are given in Table I. Test 4 was carried out with Eq. (32) (which is first-order accurate in time) used to approximate the mixed derivative $\psi_{\eta t}$. The reader may note that initially, when deformation is small, the computed field is approximately second-order accurate in time. As the magnitude of the deformation increases, the first-order approximation of the interfacial effects begins to affect the whole flow field. At $t = 2.2$ all quantities are approximately first-order accurate. Test 5 was carried out with Eq. (33) used to approximate $\psi_{\eta t}$. The results demonstrate that the algorithm delivers approximately second-order temporal accuracy at all times. Figure 22 illustrates variations of the absolute error as a function of Δt at the same test points as used in Figs. 6 and 7. It can be seen that $\Delta t = 0.3$ provides sufficient accuracy.

The timing information is based on calculations carried out from $t = 0.2$ to $t = 0.8$, with $\varepsilon_1 = 10^{-7}$ and $\varepsilon_2 = 10^{-6}$. The algorithm requires on average 125 inner iterations per one outer iteration, and 500 outer iterations for Δt_1. Similar numbers for Δt_2 were 154 and 420 and for Δt_3 were 174 and 392. If one uses the same time step for the one-step and two-step implicit algorithms, the two-step method is 1.2 times faster. If one wants to maintain

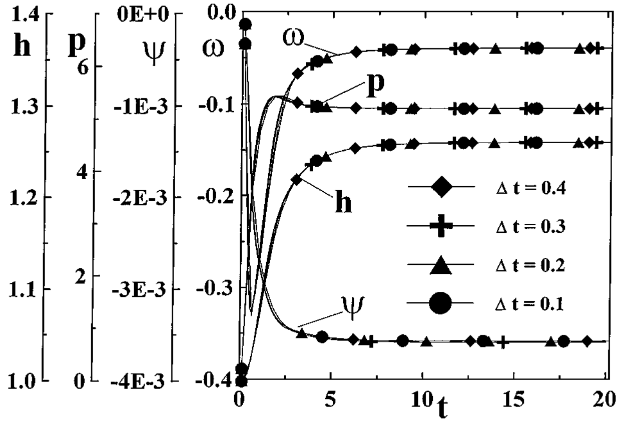

FIG. 22. Variation of ω and ψ at $(\xi, \eta) = (2.9, 0.9)$ (A) and h at $\xi = 1.5$ and p at $\xi = 2.9$ (B) as a function of Δt. Other test conditions as in Fig. 21; $\Delta\xi = \Delta\eta = 1/20$ in all calculations.

approximately the same absolute accuracy and selects, say $\Delta t = 0.1$ for the one-step method, and $\Delta t = 0.3$ for the two-step method, the later method is 2.7 times faster.

As an additional test, the case of transition from steady to oscillatory convection reported in Ref. [9] for $L = 2$, $\mathrm{Re} = 220$, $\mathrm{Ma} = 2.2$ has been investigated similarly, as in the case of the one-step implicit method (see Section 3.3.3.2.). Results obtained using the one-step and two-step methods described here agree with each other and are in agreement with those described in [9].

4. SUMMARY

A family of algorithms for analysis of the dynamics of unsteady nonisothermal capillary interfaces has been developed. The algorithms solve the unsteady free boundary problem for the Navier–Stokes and energy equations. Accurate modelling of the surface tension effects and the viscous stress at the interface is assured by implementation of the coordinate transformation method. The unknown time-dependent solution domain is mapped onto a fixed rectangular computational domain with the explicit form of the time-dependent mapping to be determined as a part of the numerical procedure. All algorithms have a similar logical structure and involve iterations between the inner and outer problems at the new time level. The inner problem consists of evaluation of the flow field for the assumed location of the interface, and the outer problem involves adjustment of the interface so that the normal stress and the kinematic conditions are satisfied. The algorithms use streamfunction-vorticity formulation for the flow variables. All spatial discretization formulas are second-order accurate. Different treatment of time derivatives lead to the one-step first-order implicit method, the second-order Crank–Nicolson and trapezoidal methods, and the two-step second-order implicit method. The Crank-Nicolson and trapezoidal methods were found to be non-self-starting (for practical applications) and subject to critical stability conditions and, thus, are not recommended. The one-step and two-step implicit methods were found to work very well for a wide range of parameter values. The two-step method is not self-starting but is about three times faster (for the same absolute accuracy) than the one-step method. Various tests have shown that the algorithms deliver the theoretically predicted accuracy, even for very large interfacial distortions.

ACKNOWLEDGMENT

The authors acknowledge the support of this work provided by the Natural Sciences and Engineering Council of Canada.

REFERENCES

1. J. M. Floryan and H. Rasmussen, Numerical methods for viscous flows with moving boundaries, *Appl. Mech. Rev.* **42**, 323 (1989).
2. C. Chen and J. M. Floryan, Numerical simulation of nonisothermal interfaces, *J. Comput. Phys.* **111**, 183 (1994).
3. F. Shokoohi and H. G. Elrod, Numerical investigation of the disintegration of liquid jets, *J. Comput. Phys.* **71**, 324 (1987).
4. F. Shokoohi and H. G. Elrod, Algorithms for Eulerian treatment of jet breakup induced by surface tension, *J. Comput. Phys.* **89**, 483 (1990).
5. C. Y. Loh and H. Rasmussen, A numerical procedure for viscous free surface flows, *Appl. Numer. Math.* **3**, 479 (1987).
6. A. Garba, A. Mofid, and R. Peyret, Spectral solution of free surface flows, *Finite Elements Anal. Design* **16**, 191 (1994).
7. I. S. Kang and L. G. Leal, Numerical solution of axisymmetric, unsteady free-boundary problem at finite Reynolds number. Finite-difference scheme and its application to the deformation of a bubble in a uniaxial straining flow, *Phys. Fluids* **30**, 1929 (1987).
8. J. C. Chen, W. C. Chen, and F. S. Hwu, Numerical computations of unsteady thermocapillary convection in a rectangular cavity with surface deformation, *Heat Transfer Metals Containerless Process. Manuf. HTD* **162**, 89 (1991).
9. J. C. Chen and F. S. Hwu, Oscillatory thermocapillary flow in a rectangular cavity, *Int. J. Heat Mass Transfer* **36**, 3743 (1993).
10. A. Rybicki and J. M. Floryan, Thermocapillary effects in liquid bridges, *Phys. Fluids* **30**, 1956 (1987).